

KfK 2832/1

Juli 1979

**Fast Rigorous
Numerical Method for the
Solution of the Anisotropic
Neutron Transport Problem
and the NITRAN System for
Fusion Neutronics Application
Part I**

A. Takahashi, D. Rusch

Institut für Neutronenphysik und Reaktortechnik

Kernforschungszentrum Karlsruhe

KERNFORSCHUNGSZENTRUM KARLSRUHE

Institut für Neutronenphysik und Reaktortechnik

KfK 2832/I

Fast Rigorous Numerical Method for the Solution of the
Anisotropic Neutron Transport Problem and the NITRAN
System for Fusion Neutronics Application

Part I

Akito Takahashi* and Detlef Rusch

* Guest scientist from Osaka University, Japan
as a research fellow of the
Alexander-von-Humboldt-Stiftung

Kernforschungszentrum Karlsruhe GmbH, Karlsruhe

Als Manuskript vervielfältigt
Für diesen Bericht behalten wir uns alle Rechte vor

Kernforschungszentrum Karlsruhe GmbH
ISSN 0303-4003

Abstract

Some recent neutronics experiments for fusion reactor blankets show that the precise treatment of anisotropic secondary emissions for all types of neutron scattering is needed for neutron transport calculations. In the present work new rigorous methods, i. e. based on non-approximative microscopic neutron balance equations, are applied to treat the anisotropic collision source term in transport equations. The collision source calculation is free from approximations except for the discretization of energy, angle and space variables and includes the rigorous treatment of nonelastic collisions, as far as nuclear data are given.

Two methods are presented: first the Ii-method, which relies on existing nuclear data files and then, as an ultimate goal, the I*-method, which aims at the use of future double-differential cross section data, but which is also applicable to the present single-differential data basis to allow a smooth transition to the new data type.

An application of the Ii-method is given in the code system NITRAN (an acronym for Non-Isotropic TRANsport) which employs the S_N -method to solve the transport equations. In general, magnetic tape is used as a storage interface to separate the scattering kernel calculations from the calculation, which solves the S_N -difference equations.

The calculational speed of the Ii-method is high, because a new analytical integration over the second angular variable is introduced into the - also new - concept of the angular transfer probability. Compared to the approximative P_L -calculations the computation time is between P_3 and P_5 . Thus, the rigorous

methods are not only valuable as reference methods, but also for technical application.

Both rigorous methods, the I_i - and the I^* -method, are applicable to all radiation transport problems and they can be used also in the Monte-Carlo-method to solve the transport problem.

Some demonstrative calculations for Li, Be and C spheres with a central D-T neutron source show that the effect of the anisotropy of the non-elastic collisions on the scalar flux and the reaction rates is very large.

A proposal is given that the double differential cross sections for each material should be given in a future nuclear data file in the form of a total neutron emission double-differential cross section, for all types of interactions together, in the laboratory system. These cross sections can be used with the more advanced, but also rigorous I^* -method.

Strenge Methoden für anisotrope Neutronentransport-Rechnungen und
das NITRAN-System für Anwendungen bei Neutronik-Rechnungen zu
Fusionsreaktoren

Zusammenfassung

Einige neuere Experimente zur Neutronenphysik des Blankets eines Fusionsreaktors zeigen, daß eine genaue Behandlung der anisotropen Sekundärneutronen-Verteilungen für alle Arten von Streuung für Neutronentransport-Rechnungen erforderlich ist. In dieser Arbeit werden neue, strenge Methoden angewendet, um die anisotrope Stoßquelle in Transportgleichungen zu behandeln. Die Berechnung des Stoßquellterms ist frei von Näherungen mit Ausnahme der Diskretisierung von Energie-, Raum- und Winkelkoordinaten und schließt die strenge Behandlung der nicht-elastischen Stöße ein.

Zwei Methoden werden vorgestellt: Zuerst die Ii-Methode, die gegenwärtig verfügbare Datensätze zu verwenden erlaubt, dann die I*-Methode als das eigentliche Ziel, die auf die Verwendung zukünftiger doppelt-differentieller Wirkungsquerschnitte ausgerichtet ist, die aber gleichwohl auf einzel-differentielle Daten zurückgreifen kann, damit ein sanfter Übergang zum neuen Datentyp möglich ist.

Eine Anwendung der Ii-Methode im Programmsystem NITRAN (ein Acronym für Nicht-Isotroper TRANsport) wird beschrieben, wobei die S_N -Methode zur Lösung der Transportgleichung benutzt wird. Ganz allgemein wird Magnetband als Zwischenspeicher eingesetzt; insbesondere, um die Berechnung des Streukerns von den Rechnungen zur Lösung der S_N -Differenzgleichungen zu trennen.

Die Rechengeschwindigkeit der Ii-Methode ist hoch, weil eine neue analytische Integration über die zweite Winkelvariable eingeführt wird in das ebenso neue Konzept einer Winkel-Übergangswahrscheinlichkeit. Verglichen mit den approximativen P_L -Rechnungen liegt die Rechenzeit zwischen P_3 und P_5 . Daher sind die strengen Methoden nicht nur als Referenz wertvoll, sondern auch für den technischen Gebrauch. Beide Methoden, die Ii- und die I*-Methode, sind anwendbar in allen Strahlungstransportproblemen. Sie können auch für die Monte-Carlo-Methode zur Lösung von Transportproblemen eingesetzt werden.

Einige Rechnungen für Kugeln aus Li, Be und C mit einer zentralen D-T-Quelle zeigen, daß der Effekt der Anisotropie der nicht-elastischen Streuung hinsichtlich der Skalarflüsse und der Reaktionsraten sehr groß ist.

Es wird vorgeschlagen, daß die doppelt-differentiellen Wirkungsquerschnitte für jedes Material in einem zukünftigen Kerndatensatz in der Form eines totalen Neutronen-Emissions-Querschnitts in doppelt-differentieller Form für alle Reaktionsarten zusammengefaßt im Laborsystem gegeben werden sollten. Diese Art von Querschnitt kann dann mit der fortgeschrittenen, aber gleichermaßen strengen I*-Methode verwendet werden.

Contents

1. Introduction
2. The Ii-method
 - 2.1 The collision source term in the neutron transport equation
 - 2.2 Character of the Ii-function
 - 2.3 Relation between the Ii- and the P_L -method
3. Realization of the Ii-method
 - 3.1 Discretized balance equation (S_N -equation)
 - 3.2 Development of the NITRAN code system and description of its structure
 - 3.3 Computational procedure in the codes
 - 3.3.1 NIO
 - 3.3.2 NIKER
 - 3.3.3 S_N -codes
4. Test calculations and results
 - 4.1 Testing the accuracy of the P_L -method and comparing the calculational speeds
 - 4.1.1 Calculational conditions
 - 4.1.2 Results for flux and reaction rate
 - 4.1.3 Calculational speed of the Ii-method
 - 4.2 Effect of the anisotropy of the non-elastic scattering
 - 4.2.1 In ${}^7\text{Li}$, referring to the lithium sphere experiment
 - 4.2.2 Effect in spheres of ${}^9\text{Be}$ and ${}^{12}\text{C}$
5. The I^* -method
 - 5.1 Double differential cross section
 - 5.2 The neutron balance equation and its collision source
 - 5.3 Relation between the I^* - and the Ii-method
 - 5.4 Discretization of the I^* -function
6. Conclusions
 - 6.1 Conclusions with respect to accomplished work
 - 6.2 Conclusions with respect to future development
7. Appendices

1. Introduction

We have met severe difficulties in the application of currently used neutron transport code systems with available evaluated nuclear data files.

Because of the localized D-T neutron source and strongly anisotropic collisions, the neutron fields become very anisotropic. Computational accuracies for angular and scalar fluxes and reaction rates become sometimes very poor, and we have had no means to estimate the accuracy of our calculation tools. Difficulties are arising from both approximative methods of calculation and insufficient nuclear data files. Commonly, the status of the data files reflects the approximations in the calculational methods. Therefore, when introducing a progress into the calculational methods, one has immediately to solve also the data problem. First in this report we present a solution (the Ii-method) for the rigorous anisotropic neutron transport calculation relying on an existing data file. Then we show the ultimate goal, the I^{*}-method, which is more general and simpler by the use of the double differential neutron emission cross section and a generalized angular transfer probability. But double differential data will only be available in the future, and so we have to show the important effects by means of the Ii-method. In order to see the present status, we pick up the 4 recent works, which contain typical results relating to the present work.

At Jülich [1,2,3,4] tritium production rate measurements were carried out in a cylindrical assembly of natural lithium. Calculations were done mainly with the Monte-Carlo code MORSE using ENDF/B-III data. There was a fair agreement between measured and calculated results. In the same

lithium assembly a beryllium layer as a neutron multiplier was used. For this case they reported a large discrepancy between experiment and calculation. The multiplication factor of the beryllium was measured independently by surrounding it with a polyethylene layer instead of the lithium assembly. There the calculated multiplication factor (MORSE with ENDF/B-IV data) was 20% higher than the measured one.

At JAERI, in Japan, they measured threshold fission rate distributions in a nearly spherical assembly of natural lithium with and without graphite reflector [5,6], and compared them with results of $S_{64}-P_5$ -calculations using the code ANISN [7] with ENDF/B-IV data processed by SUPERTOG [8]. They found 10 to 30% discrepancies in the ratios C/E (calc./exp.), see Fig. 1.

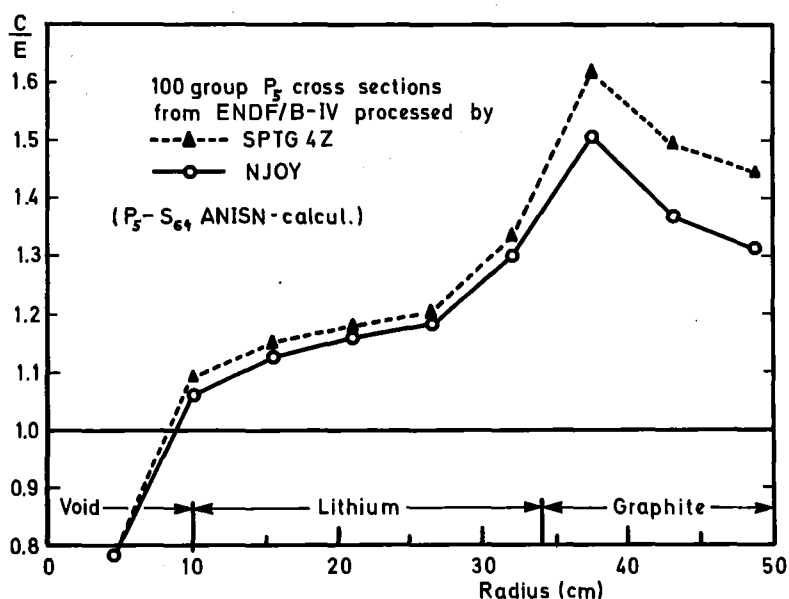
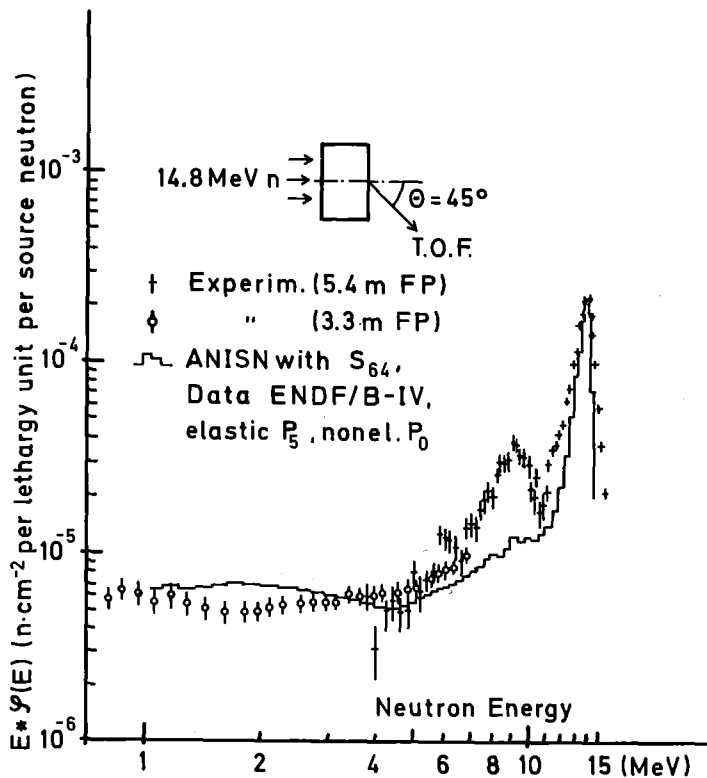


Fig. 1: Lithium experiment at JAERI: spherical assembly with reflector; rate measurements

They presumed that the effect should be due to the anisotropy of non-elastic scattering, which cannot be treated in code systems like ANISN + SUPERTOG. Some support for this hypothesis was given by the results of another calculation using the GAM-II 100 group cross section set [9] processed by NJOY [10]. This data set included the anisotropy of the inelastic scattering to the first level in carbon with a P_5 approximation. As can be seen from Fig. 1 the discrepancy between calculation and measurement is slightly reduced. Their assembly, however, was constructed with a rather high fraction of stainless steel in the lithium zone in a pseudo-spherical matrix structure, which makes the analysis complicated.

At the Osaka University, measurements of angular spectra from plane lithium assemblies based on the associated particle time-of-flight method [11,12,13] were carried out. The results were compared with S_{64} - P_5 -calculations with ANISN + SUPERTOG, using ENDF/B-IV data. They found large discrepancies in the 4 to 10 MeV range, see Fig. 2, which were attributed to the anisotropy of the inelastic scattering not included in the calculations. They also pointed out that the angular flux calculations by the S_N - P_L -method are strongly disturbed by the negative flux generation in the collision source term, as is shown in Fig. 3. The flux oscillations were found in heavy elements, too, besides a general discrepancy in the upper MeV range, see Fig. 4.

At Karlsruhe measurements of angular neutron spectra and the space dependent tritium production rate were done with a spherical assembly of natural lithium containing a minimum of stainless steel in the inner parts of the assembly [14, 15]. The calculations were performed with the code DTK in the S_N technique. A special partition of the angular coordinate, S_{19} , was



Li slab: comparison of measured and calculated angular leakage spectrum. Assembly of natural lithium, cross section $40 \times 60 \text{ cm}^2$, thickness 30 cm.

Fig. 2:

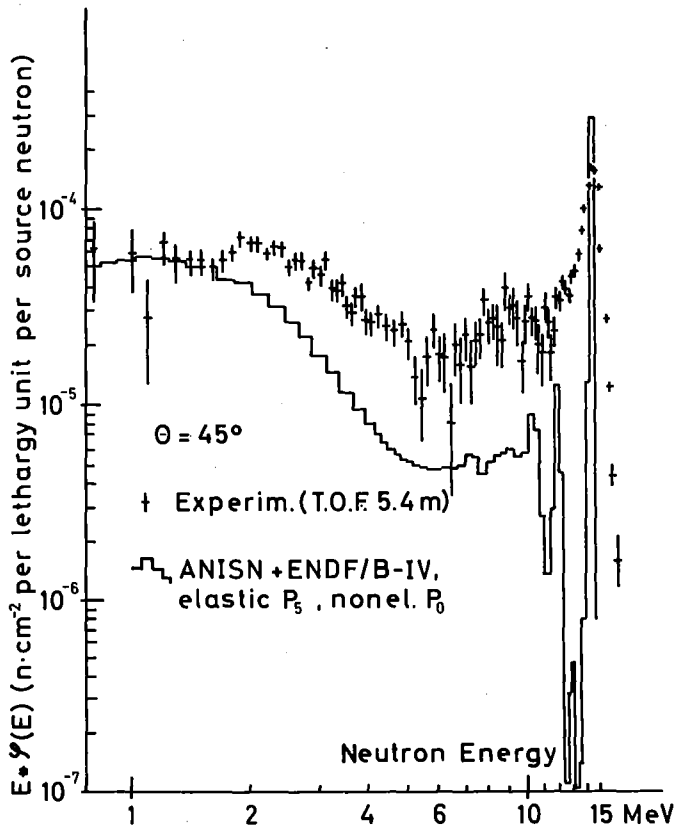
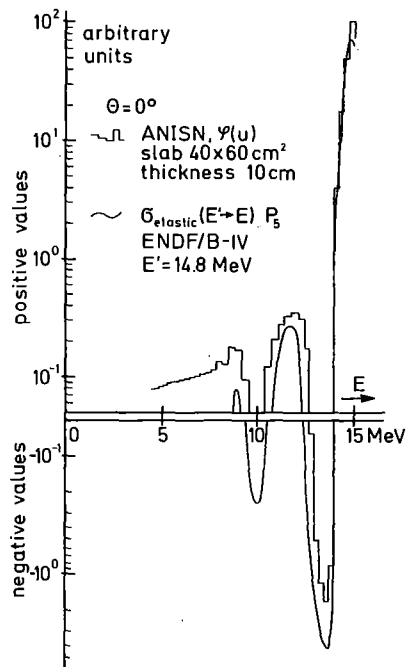


Fig. 4: Lead slab: comparison of measured and calculated angular leakage spectrum. Assembly of nat. lead, cross section $40 \times 40 \text{ cm}^2$, thickness 10 cm.



Comparison of flux and P_5 kernel for Li showing the generation of flux oscillations and negative fluxes by the P_L method

Fig. 3:

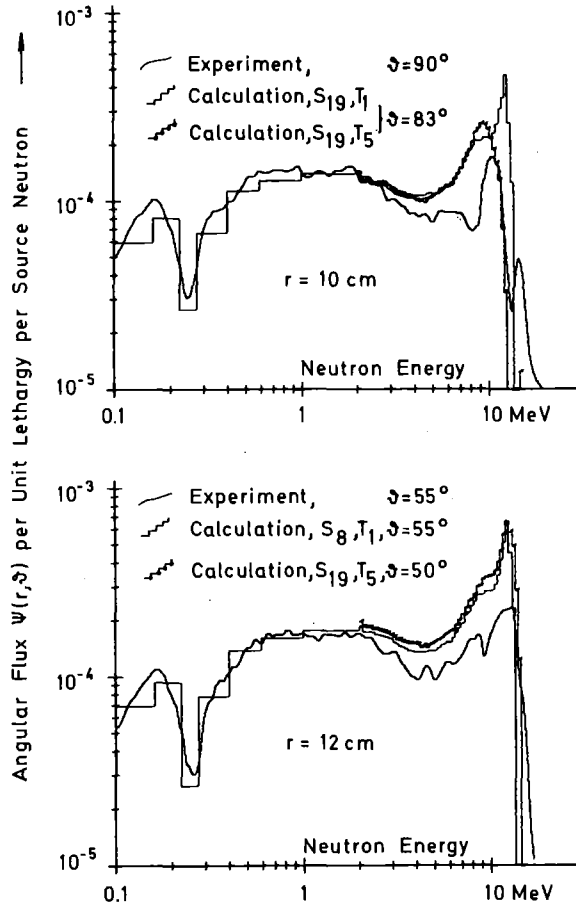


Fig. 5: Measured and calculated angular neutron spectra from a Li sphere. Calculations with measured source spectrum.

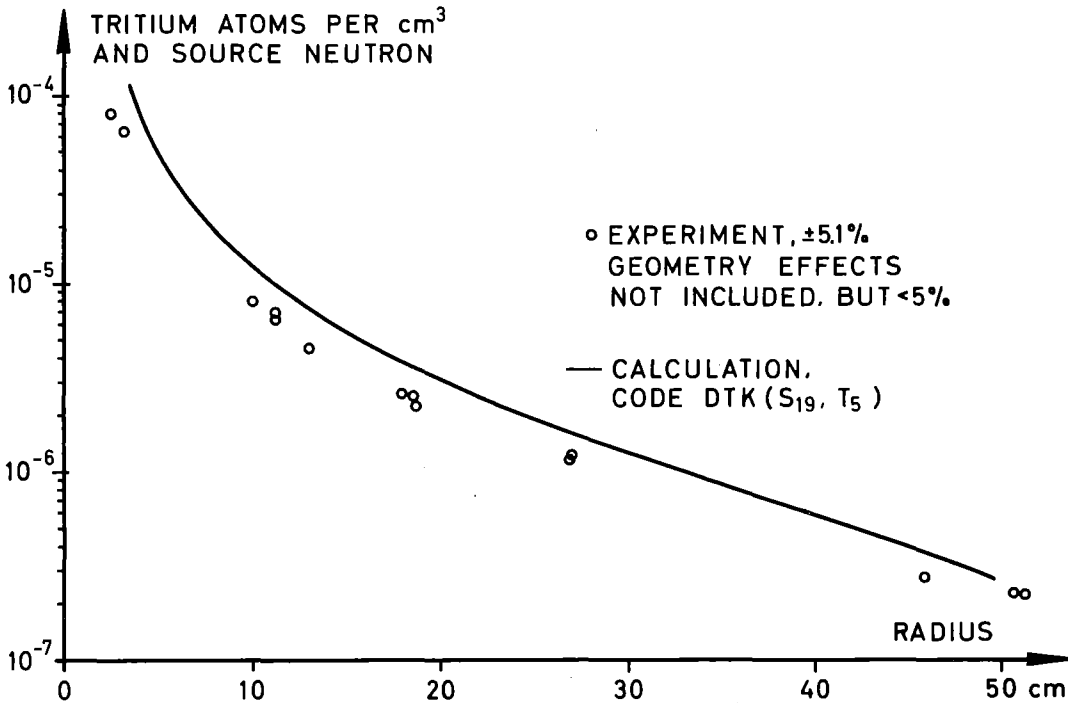


Fig. 6: Measured and calculated tritium production rates vs. radial distance from the centre of the sphere.

introduced to allow for the strong anisotropy of the neutron flux in the radial direction. For the treatment of the anisotropy of the elastic scattering a new technique of consistent improved extended transport approximation, T_5 , was used [16]. Nuclear data were ENDF/B-III for lithium and KEDAK-3 for iron. Large discrepancies in the angular fluxes under oblique directions, as shown in Fig. 5, together with a fair agreement in the radial direction lead to the conclusion, that the scalar fluxes, which could not be measured in that experiment, are calculated drastically too high in the energy range 2 to 10 MeV. The estimated discrepancy in the scalar spectra (40 to 60%) should affect the calculated tritium production by 13 to 20%. However, the discrepancy between the measured and calculated tritium production rates (Fig. 6) was larger than that. Therefore they concluded that there were two major sources of errors, namely the error of the transport calculation and the error in the ${}^7\text{Li}(n,n'\alpha)$ cross section value at 14 MeV. Lacking the possibility of including the anisotropy of the nonelastic scattering in the calculations, they were not able to verify the magnitude of the effect of the anisotropy of the nonelastic scattering.

From the above four experimental studies we may extract the following two statements:

- 1) Due to the finite Legendre polynomial expansion for the collision source term of the S_N -calculation the angular information is distorted. Errors from this have not been estimated. A rigorous reference method to validate the existing methods is therefore desirable.

2) The full anisotropy of the scattering (i. e. elastic, inelastic, (n,2n), (n,n'x), etc.) must be included in order to fulfill the need for a reference method.

As already stated, the data problem is an obstacle on the way to the goal of the desired reference method. Instead of touching existing codes, which due to their complexity would have built up additional obstacles, a completely independent code system NITRAN (an acronym for Non-Isotropic TRANsport) was developed. The code system is described in detail, as well as the result of calculations for spherical assemblies of ${}^7\text{Li}$, ${}^9\text{Be}$, and ${}^{12}\text{C}$, which prove the necessity of the rigorous method.

Finally, we will describe the I^* -method, which is also rigorous, but simpler and more general than the I_i -method. The I_i -method fits to the present status of nuclear data files, while the I^* -method will fit to the future nuclear data files that contain double differential neutron emission cross sections [17].

2. The Ii-method

2.1 The collision source term in the neutron transport equation

A purely mathematical derivation of the Ii-method is presented in a separate report [18]. Here we present it more from a physicist's point of view.

The neutron balance equation for the angular flux $f_g(\vec{r}, \vec{\Omega})$ of the energy group g is generally written as *)

$$\vec{\Omega} \cdot \vec{\nabla} f_g(\vec{r}, \vec{\Omega}) + \sigma_t^g \cdot f_g(\vec{r}, \vec{\Omega}) = (\text{collision source})_g + (\text{external source})_g \quad (1)$$

By using the new concept of an angular transfer probability for specified type of collision, i , (see Appendix 1 and ref.10) the collision source term is written as follows; by directly carrying out the integration over the second angle φ' for the collision source term with delta-functional kernels we obtain:

$$\begin{aligned} (\text{coll. source})_g = & \sum_{g'} \int_{-1}^{+1} \sum_{i=1}^{IL} \sigma_i^0(g', g) \cdot I_i(\mu', \mu) \cdot f_{g'}(\vec{r}, \mu', \varphi + \Delta_i^*) d\mu' + \\ & + \frac{1}{2} \sum_{g'} \sigma_{\text{con}}^0(g', g) \cdot \frac{1}{2\pi} \int_0^{2\pi} \int_{-1}^{+1} f_{g'}(\vec{r}, \mu', \varphi') d\mu' d\varphi' \end{aligned} \quad (2)$$

with $\mu' = \text{cosine of the incident neutron angle,}$

$\mu = \text{cosine of the outgoing neutron angle.}$

$IL = \text{total number of type of collisions (el. plus inel. level)}$

*) Throughout the text " σ " is used for macroscopic cross sections to distinguish from the summing symbol.

The first term of the right hand side of Eq. (2) shows the contribution of anisotropic collision events, while the second shows that of isotropic events in the LAB system. We need not carry out an integration of the anisotropic collision source over φ in the transport calculation^{*}). This is a merit of the Ii-method. The matrix $\sigma_i^0(g';g)$, which represents the energy distribution of secondary neutrons in the LAB system, is defined by

$$\sigma_i^0(g',g) = \sigma_i(E_{g'}, \mu_{ci}^*) \cdot g_i(E_{g'}) \quad (3)$$

where $\sigma_i(E_{g'}, \mu_{ci}^*)$ is the angular differential cross section in the CM system, and $g_i(E_{g'})$ is a Jacobian (see Appendix 2).

The Jacobian is given as follows:

$$g_i(E_{g'}) = \frac{2}{(1-\alpha) \cdot E_{g'} \cdot \sqrt{1 - Q_i/E^*}} \quad (4)$$

where

$$\alpha = (A-1)^2/(A+1)^2 \quad \text{with } A = \text{mass of nucleus relative to neutron} \quad (5)$$

$$E^* = \frac{A}{A+1} \cdot E_{g'} \quad (6)$$

$Q_i = Q$ -value for the collision of type i , with
 $Q_i = 0$ for elastic scattering

The relation between μ_{ci}^* , the cosine of the angle of the secondary neutron in the CM system, and the energies $E_{g'}$ (incident) and E_g

^{*}) The collision source for an isotropic scattering (second term of Equ. (2)) is related to the scalar flux $\Phi_g(r)$ only, because

$$\Phi_g(\vec{r}) = \int_0^{2\pi+1} \int_{-1}^1 f_g(\vec{r}, \mu, \varphi) d\mu d\varphi$$

(outgoing), derived from the scattering kinematics (see Appendix 2)

is as follows:

$$\mu_{ci}^* = \left\{ \frac{(A+1)^2}{2A} \cdot \frac{E_g}{E_g'} - \frac{A}{2} \cdot \left(1 - \frac{Q_i}{E^*} \right) - \frac{1}{2A} \right\} / \sqrt{1 - Q_i/E^*} \quad (7)$$

The matrix $\sigma_{\text{con}}^0 (g', g)$ in the second component of Eq. (2) represents the energy distribution of secondary neutrons, which is treated as isotropic in the LAB system.

The phase shift in the \mathcal{P} -space after the collision, Δ_i^* , see Fig. 7 for definitions, is given by

$$\Delta_i^* = \arccos \left(\frac{\mu_i^* - \mu\mu'}{\sqrt{1-\mu^2} \cdot \sqrt{1-\mu_i'^2}} \right) \quad (8)$$

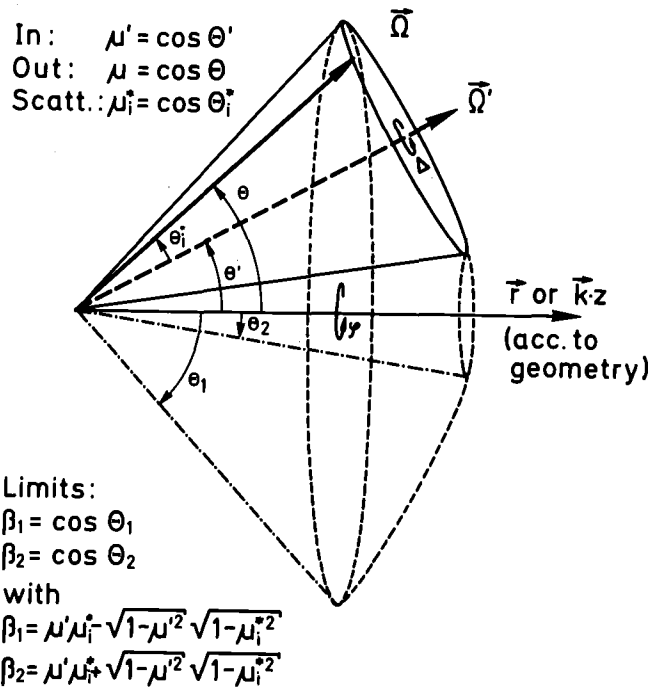


Fig.7: Definitions of angles in the LAB system.

μ_i^* , the cosine of the scattering angle in the LAB system, is given by the kinematics [18] for a type i of collision as

$$\mu_i^* = \left\{ (A+1) \cdot \sqrt{\frac{E_g}{E_g'}} - \frac{1}{A+1} \sqrt{\frac{E_g'}{E_g}} \cdot (A^2(1 - \frac{Q_i}{E_g^*}) - 1) \right\} / 2 \quad (9)$$

For given μ' and μ the phase shift ($\varphi - \varphi'$) must be fixed, because the cosine of the scattering angle μ_i^* is fixed. μ_i^* being the cosine of the angle between the $\vec{\Omega}$ and the $\vec{\Omega}'$ vectors, there is only one incident vector $\vec{\Omega}'$ corresponding to the outgoing $\vec{\Omega}$. The angular transfer probability function, the explicit use of which is new in neutron transport calculations, can be given analytically, except for some extreme cases, as

(Appendix 1):

$$I_i(\mu', \mu) = \frac{1}{\pi \sqrt{1 - \mu^2 - \mu'^2 - \mu_i^{*2} + 2\mu\mu'\mu_i^*}} \quad \text{for } \beta_1 < \mu < \beta_2 \quad (10)$$

or = 0 for $\mu \leq \beta_1$ and $\mu \geq \beta_2$,

where the limits between the kinematically allowed and forbidden regions of μ are

$$\beta_1 = \mu'\mu_i^* - \sqrt{1 - \mu'^2} \cdot \sqrt{1 - \mu_i^{*2}} \quad (11)$$

$$\beta_2 = \mu'\mu_i^* + \sqrt{1 - \mu'^2} \cdot \sqrt{1 - \mu_i^{*2}} \quad (12)$$

The physical meaning of the $I_i(\mu', \mu)$ -function and some examples are explained in the next section.

In the case of a one-dimensional transport problem we can eliminate the phase shift Δ_i^* using the symmetry condition in the φ -space. For

the spherical case, for instance, the balance equation becomes

$$\begin{aligned} & \frac{\mu}{r^2} \cdot \frac{\partial}{\partial r} (r^2 F_g(r, \mu)) + \frac{1}{r} \frac{\partial}{\partial \mu} [(1-\mu^2) F_g(r, \mu)] + \Sigma_t^g \cdot F_g(r, \mu) = \\ & = \sum_{g'} \int_{-1}^{+1} \sum_{i=1}^{IL} \Sigma_i^o(g', g) \cdot I_i(\mu', \mu) \cdot F_{g'}(r, \mu') d\mu' + \\ & + \frac{1}{2} \sum_{g'} \Sigma_{con}^o(g', g) \int_{-1}^{+1} F_{g'}(r, \mu') d\mu' + S_g(r, \mu) \end{aligned} \quad (13)$$

where:
$$F_g(r, \mu) = \int_0^{2\pi} f_g(\vec{r}, \vec{\Omega}) d\varphi,$$

$$\mu = \vec{r} \cdot \vec{\Omega} / r,$$

$S_g(r, \mu)$ the external source,

and the scalar flux $\Phi_g(\vec{r})$ is given by

$$\Phi_g(\vec{r}) = \int_{-1}^{+1} F_g(r, \mu) d\mu = \int_{-1}^{+1} \int_0^{2\pi} f_g(\vec{r}, \vec{\Omega}) d\varphi d\mu.$$

2.2 Character of the Ii-function

The Ii-function is the distribution function for the probability, with which a neutron incident at the angle*) μ' appears at an outgoing angle μ after a collision of type i with the scattering angle μ_i^* . If the scattering in the CM system is isotropic, $\sigma_i^o(g', g)$ becomes constant with re-

*) For abbreviation we use the word "angle" also for the cosines, if the distinction is easy.

spect to g , and the anisotropy of the scattering kernel is represented by the $Ii(\mu', \mu)$ -function alone. Hence, the Ii -function contains the CM-to-LAB system transformation.

As can be seen in Fig. 7 the angle vector $\vec{\Omega}$ after the collision draws a circle around the axis $\vec{\Omega}'$ of the incident vector. In the case of Ω' -symmetry this circle rotates about the position vector \vec{r} . All outgoing vectors are distributed on this curved surface. Inside a cone with opening angle θ_2 and outside a cone with opening angle θ_1 there are no outgoing vectors: this is the kinematically forbidden region. The region between θ_1 and θ_2 , resp. the cosines β_1 and β_2 , is the allowed region, and the distribution function of vectors on this curved surface is $Ii(\mu', \mu)$. The relations (11) and (12) are just the transcribed addition theorems for the cosine:

$$\beta_1 = \cos \theta_1 = \cos (\theta' + \theta_1^*) = \cos \theta' \cos \theta_1^* - \sin \theta' \sin \theta_1^*$$

$$\beta_2 = \cos \theta_2 = \cos (\theta' - \theta_1^*) = \cos \theta' \cos \theta_1^* + \sin \theta' \sin \theta_1^*$$

If the scattering angle θ_1^* becomes 0 or π , i. e. $\mu_1^* = \pm 1$, the allowed angular interval collapses to a point. In this case the Ii -function becomes a delta-function [18].

Fig. 8 shows some representative examples of angular transfer probabilities $Ii(\mu', \mu)$. The Ii -representation of the angular transfer probability is rigorous in the sense, that the scattering law is treated without approximation. For the validity of the scattering law itself in the energy range of interest no doubt has been raised so far.

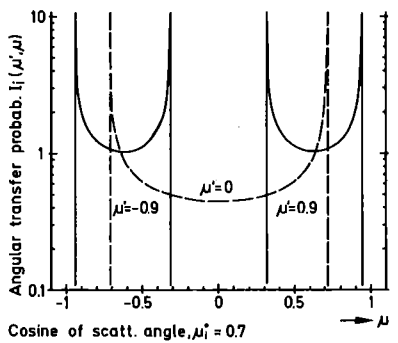
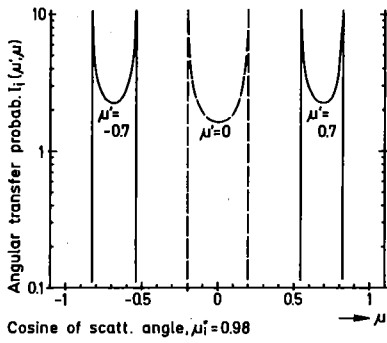
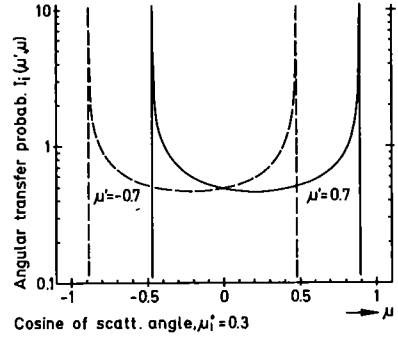
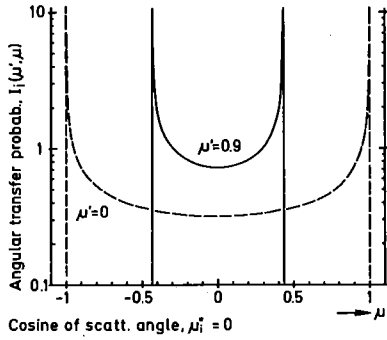


Fig. 8: Representative examples for the angular transfer probability function $I_i(\mu', \mu)$. The upper graphs contain two examples each, the lower three.

It is the most important aspect of the Ii-function that the outgoing angle μ is restricted to the region of $\beta_1 < \mu < \beta_2$. This restriction is missed in currently used approximative methods like the P_L representation of the collision source term, in which the full range of μ , i. e. $-1 \leq \mu \leq +1$, is always used. The second important point is that the angular transfer probability depends on the type of the collision through μ_i^* . This means that we have to treat the scattering kinematics for each type of collision separately in order to reconstruct the correct anisotropy of the scattering. The Ii-function satisfies the conservation of probability,

$$\int_{-1}^{+1} \bar{I}i(\mu', \mu) d\mu = \int_{\beta_1}^{\beta_2} \bar{I}i(\mu', \mu) d\mu = 1, \quad (14)$$

and is symmetric for the three variables μ', μ and μ_i^* .

2.3 Relation between the Ii- and the P_L -method

The balance equation for anisotropic neutron transport is usually written [7, 16, 19] with use of the collision source term in the form of a finitely truncated Legendre polynomial expansion:

$$\begin{aligned} & \frac{\mu}{r^2} \cdot \frac{\partial}{\partial r} [r^2 F_g(r, \mu)] + \frac{1}{r} \frac{\partial}{\partial r} [(1-\mu^2) F_g(r, \mu)] + \Sigma_t^g F_g(r, \mu) \\ & = \sum_{g'} \int_{-1}^{+1} \frac{1}{2} \sum_{\ell=0}^L \sigma^\ell(g', g) \cdot P_\ell(\mu') \cdot P_\ell(\mu) \cdot F_{g'}(r, \mu') d\mu' \\ & \qquad \qquad \qquad + S_g(r, \mu) \end{aligned} \quad (15)$$

If we take into account the kinematics of the various types of collisions, the P_L -coefficients of the matrices (the " P_L -kernels"), are given by (see also Appendix 2):

$$\sigma^0(g',g) = \sum_{i=1}^{IL} \sigma_i(E_{g'}, \mu_{ci}^*) \cdot g_i(E_{g'}) + \sigma_{con}^0(g',g) \quad (16)$$

and

$$\sigma^L(g',g) = \sum_{i=1}^{IL} (2l+1) \cdot \sigma_i(E_{g'}, \mu_{ci}^*) \cdot g_i(E_{g'}) \cdot P_l(\mu_i^*) \quad (17)$$

with $l = 1, 2, \dots, L$

The averaging within the energy groups is abbreviated for simplicity. By substituting Eqs. (16) and (17) into (15) and using Eq. (3) we get

$$\begin{aligned} (\text{Coll. source})_g &= \\ &= \sum_{g'} \int_{-1}^{+1} \sum_{i=1}^{IL} \sigma_i^0(g',g) \cdot \left[\frac{1}{2} \sum_{l=0}^L (2l+1) \cdot P_l(\mu_i^*) \cdot P_l(\mu') \cdot P_l(\mu) \right] \\ &\quad \cdot F_{g'}(r, \mu') d\mu' + \frac{1}{2} \sum_{g'} \sigma_{con}^0(g',g) \int_{-1}^{+1} F_{g'}(r, \mu') d\mu'. \end{aligned} \quad (18)$$

Comparing Eq. (18) with Eq. (13) we find that the angular transfer probability $P_i^L(\mu', \mu)$ for a collision of the type i is expressed by

$$P_i^L(\mu', \mu) = \frac{1}{2} \sum_{l=0}^L (2l+1) \cdot P_l(\mu_i^*) \cdot P_l(\mu') \cdot P_l(\mu). \quad (19)$$

In ref. [18] it is proved that the function $P_i^L(\mu', \mu)$ converges against $\bar{I}_i(\mu', \mu)$, if $L \rightarrow \infty$, i. e.

$$\bar{I}_i(\mu', \mu) = \frac{1}{2} \sum_{l=0}^{\infty} (2l+1) \cdot P_l(\mu_i^*) \cdot P_l(\mu') \cdot P_l(\mu). \quad (20)$$

In Appendix 3 the same is done for the I^* -method.

Thus it is demonstrated from another point of view that the Ii-method is a rigorous treatment of the anisotropic collision source term.

A first impression of the difference between the P_L - and the Ii-method is given by Fig. 9, which shows angular transfer probability functions with various finite truncations of the Legendre polynomial expansion in comparison with the rigorous Ii-function. The P_5 approximation is still very rough from this point of view. More than 20 terms of the Legendre expansion are needed for a representation of the shape of the Ii-function. Rigorous angular transfer probabilities are in most cases unsymmetric against $\mu = 0$. Thus, it can be seen from Fig. 9, why the P_L -approximation with low even number of L (i. e. P_2 or P_4) is less accurate than that for odd L (i. e. P_1 , P_3 or P_5).

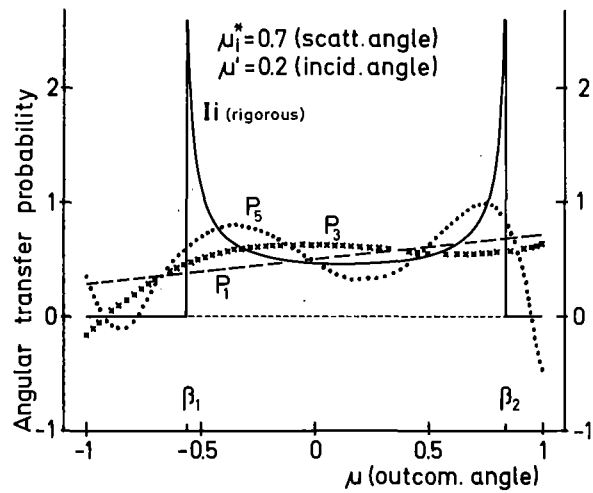
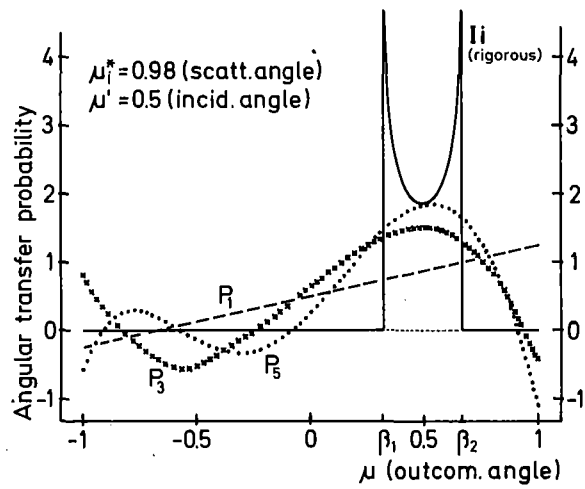


Fig. 9a: Angular transfer function $I_i(\mu', \mu)$ and its approximation by the P_L method at lower orders

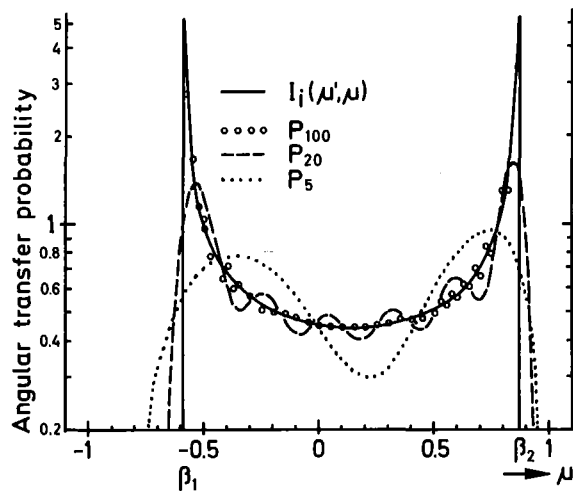


Fig. 9b: Angular transfer function $I_i(\mu', \mu)$ for $\mu' = 0.2$, $\mu_i^* = 0.682$, and its approximation by the P_L method at higher orders

3. Realization of the li-method

3.1 Discretized balance equation (S_N -equation)

The discrete ordinates equation based on Eq. (13) is derived by discretization of the r and μ variables [19] for the spherical geometry:

$$\begin{aligned} & w_n \mu_n \left[A_{m+\frac{1}{2}} \cdot F_g(m+\frac{1}{2}, n) - A_{m-\frac{1}{2}} \cdot F_g(m-\frac{1}{2}, n) \right] + \\ & + \alpha_{n+\frac{1}{2}} \cdot F_g(m, n+\frac{1}{2}) - \alpha_{n-\frac{1}{2}} \cdot F_g(m, n-\frac{1}{2}) + \\ & + w_n G_t^g \bar{V}_m F_g(m, n) = w_n \bar{V}_m (C_g + S_g) \end{aligned} \quad (21)$$

The notation follows ref. [19]:

μ_n : angle point; $\mu_n \pm \frac{1}{2}$: angular boundaries

w_n : weight for angle point

$$A_{m \pm \frac{1}{2}} = 4 \pi \cdot (r_{m \pm \frac{1}{2}})^2 \cdot ; \text{ area of cell surfaces} \quad (22)$$

$r_{m \pm \frac{1}{2}}$; radial points at radial boundaries of volume cell.

$$\alpha_{m, n+\frac{1}{2}} - \alpha_{m, n-\frac{1}{2}} = - w_n \mu_n (A_{m+\frac{1}{2}} - A_{m-\frac{1}{2}}) \quad (23)$$

$$\alpha_{m, n_{\max}+\frac{1}{2}} = \alpha_{m, \frac{1}{2}} = 0 \quad (\mu = \pm 1) \quad (24)$$

$$\bar{V}_m = 4 \pi (r_{m-\frac{1}{2}}^3 - r_{m+\frac{1}{2}}^3) / 3; \text{ volume of the cell} \quad (25)$$

C_g ; collision source for energy group g

S_g ; external source for energy group g

$F_g(m \pm \frac{1}{2}, n)$; angular fluxes at spatial boundaries of a volume cell

$F_g(m, n \pm \frac{1}{2})$; angular fluxes at angular boundaries of a space-angle volume cell

$F_g(m, n)$; angular flux at a midpoint of the volume cell

The new formulation for the collision source term is the essential change to the S_N -method.

$$C_g(m, n) = \sum_{g'} \sum_{n'} \sigma_g(g'; n', n) \cdot F_{g'}(m, n') \cdot w_{n'} + \sum_{g'} \sigma_{con}^o(g', g) \cdot \sum_{n'} [F_{g'}(m, n') \cdot w_{n'}], \quad (26)$$

where the anisotropic scattering kernel (matrix) $\sigma_g(g'; n', n)$ is given by

$$\sigma_g(g'; n', n) = \sum_{i=1}^{IL} \sigma_i^o(g', g) \cdot T_i(n', n). \quad (27)$$

The angular transfer probability $Ii(\mu', \mu)$ is discretized into $T_i(n', n)$ by averaging $Ii(\mu', \mu)$:

$$T_i(n', n) = \frac{1}{4w_{n'}w_n} \int_{\mu_{n'} - \Delta\mu_{n'-\frac{1}{2}}}^{\mu_{n'} + \Delta\mu_{n'+\frac{1}{2}}} \int_{\mu_n - \Delta\mu_{n-\frac{1}{2}}}^{\mu_n + \Delta\mu_{n+\frac{1}{2}}} Ii(\mu', \mu) d\mu d\mu', \quad (28)$$

the indices of $\Delta\mu_{n\pm\frac{1}{2}}$ indicating asymmetric intervals.

From Eq. (10) we obtain *)

$$T_i(n', n) = \frac{1}{4w_{n'}w_n} \int_{\mu_{n'} - \Delta\mu_{n'-\frac{1}{2}}}^{\mu_{n'} + \Delta\mu_{n'+\frac{1}{2}}} [\arcsin(y_{n+\frac{1}{2}}) - \arcsin(y_{n-\frac{1}{2}})] d\mu' \quad (29)$$

$$*) \quad 2w_n \cdot T_i(n', n) = \int_{\mu_n - \Delta\mu_{n-\frac{1}{2}}}^{\mu_n + \Delta\mu_{n+\frac{1}{2}}} Ii(\mu', \mu) d\mu_n =$$

$$= \frac{1}{\pi} \int_{y_{n-\frac{1}{2}}}^{y_{n+\frac{1}{2}}} \frac{1}{\sqrt{1-y^2}} dy = \frac{1}{\pi} [\arcsin(y_{n+\frac{1}{2}}) - \arcsin(y_{n-\frac{1}{2}})]$$

for $\beta_1 < \mu_n < \beta_2$
with $y_{n\pm\frac{1}{2}}$ see overleaf.

where

$$y_{n \pm \frac{1}{2}} = \frac{\mu_{n \pm \frac{1}{2}} - \mu_n \mu_i^*(g', g)}{\sqrt{1 - \mu_n^2} \cdot \sqrt{1 - \mu_i^{*2}}} \quad (30)$$

In the present code (FUNCII, see section 3.3) averaging over w_n , is not done. Eq. (29) is approximated by

$$T_i(n', n) = \frac{1}{2\pi w_n} \left[\arcsin(y_{n+\frac{1}{2}}) - \arcsin(y_{n-\frac{1}{2}}) \right] \quad (31)$$

for $\beta_1 < \mu_n < \beta_2$.

As the μ_n variables must be between β_1 and β_2 , some provisions are needed for the case that β_1 or β_2 is included in the mesh w_n (see Appendix FUNCII). One can notice, however, that the analytical integrability is advantageous for the discretization.

3.2 Development of the NITRAN code system and description of its structure

The new Ii-method can be applied to currently used S_N code systems like DTK [20] or ANISN [7] by rearranging their cross section processing codes GRUCAL [21] and SUPERTOG [8], to stay with the first two examples. Parts of the collision source calculation must be changed in the S_N codes. This, however, is not an easy task, because the nuclear data processing and the kernel production are tightly connected to the S_N calculation schemes. For instance, about 10 essential subroutines like OUTER and INNER in DTK [20] must be revised in order to apply the Ii-method.

Therefore we decided to develop an independent code system NITRAN ,*) which has a new manner of data processing and scattering kernel calculation, based on the Ii-method. Fig. 10 depicts the concept of the NITRAN system. The neutron transport calculation itself, i. e. the solution of the S_N equations is separated from the kernel calculations. This concept differs from the currently used scheme, in which the scattering matrices are produced together with the calculation on the solution of the S_N equations, even if a calculation on the same material is repeated. The nuclear data file KEDAK [20,23] is used as a nuclear data source. Auxiliary input for nuclear data is necessary, because some of the data needed for the new type of calculation are presently not available from KEDAK.

In addition to Fig. 10, Fig. 11 shows the working scheme of the kernel calculation. The first processing code NIO produces the the so-called P_0 -kernel $\sigma_1^0(g',g)$ with use of the scattering kinematics and the differential cross sections, and stores it on magnetic tape No. 1. These scattering matrices can already be used for transport calculations with isotropic collision source. The second processing code NIKER produces anisotropic scattering matrices $\sigma_g(g';n'n)$ by means of the Ii-function, and stores them on magnetic tape No. 2. This processing is done for each isotope. The interface code NIMIX produces the anisotropic scattering matrices for materials with several isotopes and for several layers of materials ("zones"). Its results are stored on magnetic tape No. 3. The code NIMIX is not yet realized.

*) Non-Isotropic TRANsport

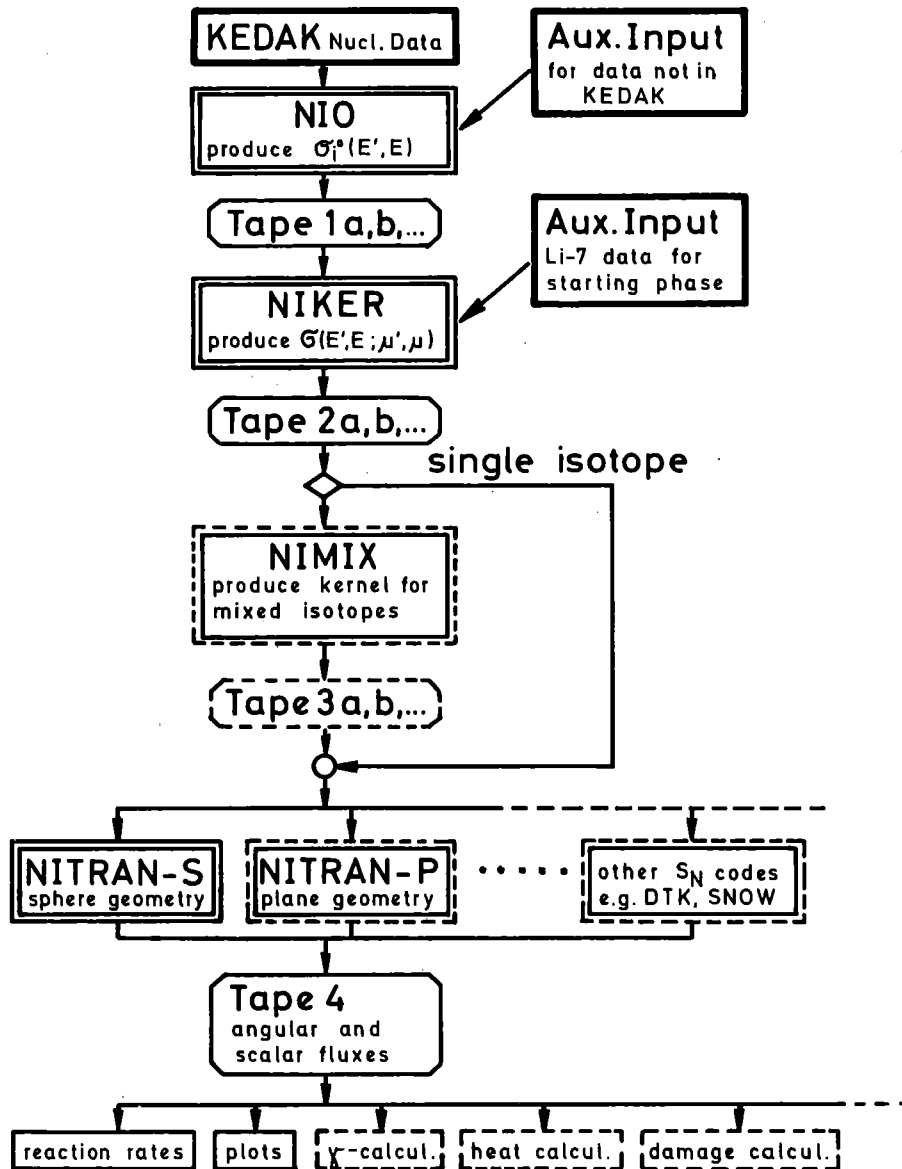


Fig. 10: Concept of the NITRAN System

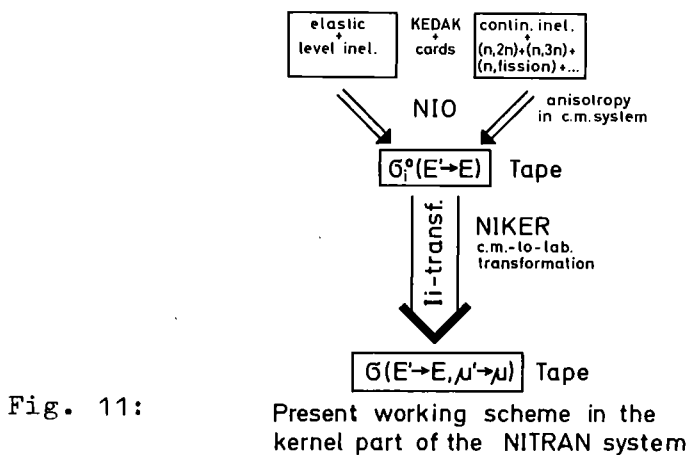


Fig. 11:

Present working scheme in the kernel part of the NITRAN system

Transport calculations can be done by means of various S_N -codes. When writing this report, only the one-dimensional code NITRAN-S for spherical geometry is completed. S_N -codes for other geometries are planned, but they are not necessary for the demonstration of the new method. Angular and scalar fluxes, as calculated by the various S_N -codes, are stored on magnetic tape No. 4, where they are ready for use in subsequent calculations of nuclear effects and for γ -transport.

The working scheme of the kernel calculation reflects the situation with the nuclear data file. At present, scattering anisotropies in the CM system are treated for elastic and level-inelastic scattering only. Angular distributions for the secondary neutrons of elastic scattering are read from KEDAK, whilst the data for inelastic level scattering have to be read from cards. Continuum-inelastic and (n,2n) scattering are treated as isotropic in the CM system and $\sigma_{\text{con}}^0(g',g)$ is produced with use of the evaporation model. In future the first emitted neutron from the (n,2n) process should be, at least, treated as anisotropic in the CM system. This can be treated by the same kinematics as the level-inelastic scattering. Then the second neutron may be approximated as isotropic in the CM system. In the same way also the anisotropy of processes like (n,n'x) and (X,n'x') should be included, too.

Anisotropic scattering matrices are produced by NIKER by summing up $\sigma_i^0(g',g) \cdot I_i(\mu',\mu)$ - or, more accurately: $\sigma_i^0(g',g) \cdot T_i(n',n)$ - for all types i of scattering: elastic, level-inelastic and continuum. In the following some explanations on details of the calculational procedures are given.

3.3 Computational procedures in the codes

3.3.1 NIO

In Fig. 12 the calculational flow in NIO is demonstrated for the case of elastic scattering on ${}^7\text{Li}$. A 67 group structure (see Table 1) is used for all calculations in this report. The energy of the secondary neutrons after elastic scattering spreads over 22 of these groups. First we search the energy points E_g , on which the secondary neutron energy spreads, according to ref. [18], between

$$E_{\max} = E_{g'} \cdot \frac{A^2(1 - Q_i/E^*) + 2A\sqrt{1 - Q_i/E^*} + 1}{(A+1)^2} \quad (32)$$

$$E_{\min} = E_{g'} \cdot \frac{A^2(1 - Q_i/E^*) - 2A\sqrt{1 - Q_i/E^*} + 1}{(A+1)^2} \quad (33)$$

Secondly we transform the E_g -points to the cos-angle points μ_c in the CM system with use of Eq. (7) - step 1 to 2 in Fig. 12. Then we can pick up angular distribution data corresponding to $\mu_{ci} = \mu_c(E_g)$ points. Thirdly we transform the angular distribution data into an E_g array (step 2 to 3 in Fig. 12, backwards), and integrate them over E_g (which in effect is made by summing up) to get SUM. SUM should be the Jacobian $g_i(E_{g'})$ of Eq. (3). In the actual calculation, however, we normalize SUM to the cross section $\sigma_i(E_{g'})$ instead of using the $g_i(E_{g'})$ factor. Thus, we obtain $\sigma_i^0(g',g)$. The averaging within the groups is done with use of a subdivision in each energy group, for the example of ${}^7\text{Li}$ the groups were subdivided into about 10 groups. This scheme is repeated for the level inelastic scattering. As can be seen from Eqs. (32) and (33), if E^* approaches the maximum possible value $E^* = Q_i$,

we get $E_{\min} = E_{\max} = E_g / (A+1)^2$, which is the energy of the neutron stuck to the nucleus. Above the related incident neutron energy of $E_g = E_f = Q_i \cdot (A+1) / A$ we get a separate scattered neutron. At the slightly higher value of $E_g = E_b = Q_i \cdot A / (A-1)$ we get $E_{\min} = 0$. Above this value of E_g , we have neutrons scattered into the backward direction of the LAB system ($\mu_i^* < 0$). Therefore this value E_b is called the backward threshold [33]. Below E_b the scattered neutrons appear inside a forward cone, the opening angle of which shrinks from $\mu = 0$ to $\mu = 1$, as E_g approaches E_f , which is called the forward threshold. Inside the forward cone the energy of the outgoing neutron has

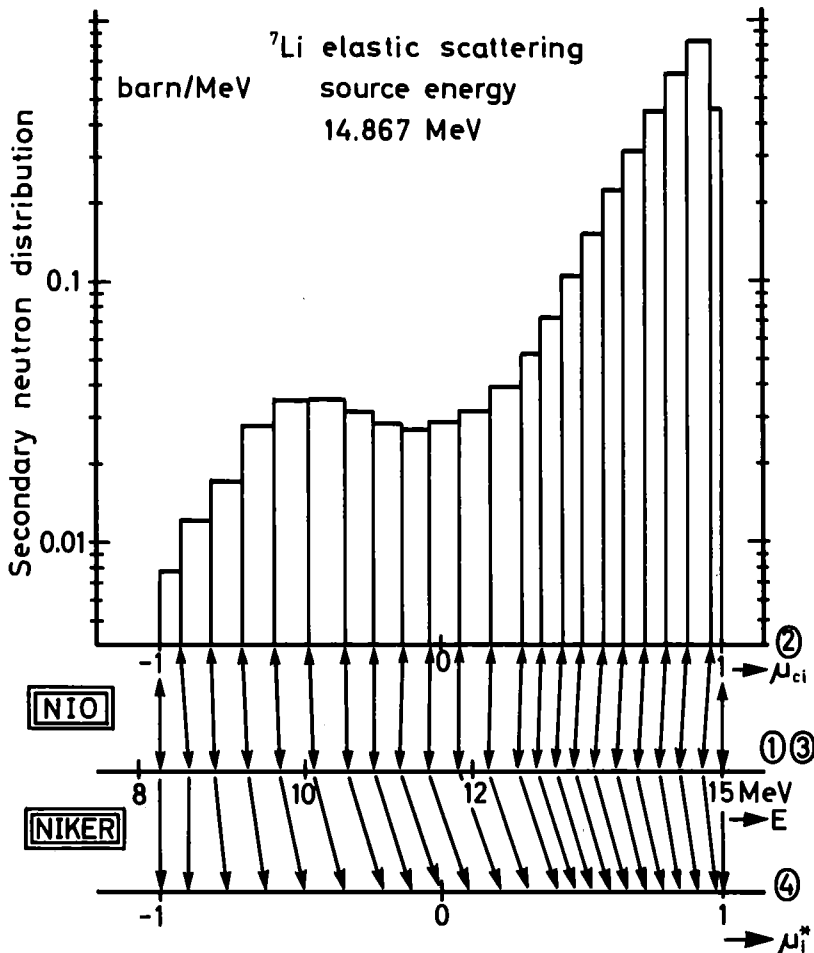


Fig. 12: Flow of the scattering kernel production in the NITRAN system, ① → ② → ③ → ④

two possible values. At present the programs account only for one of the two values. This simplification affects only one or two groups of incident neutron energy in the present 67-group structure (see table 1 at the end of the paper) and, moreover, the related cross sections are small.

A simplified flow chart of NIO is shown in Fig. 13. Flow charts of some subroutines, which are essential in the Ii-method, are shown in Fig. 14. We first open the KEDAK file with use of LDFOPN, which belongs to the KEDAK retrieval package [23]. The subsequent use of the other retrieval routines is omitted in Fig. 13. These direct-access routines are called from subroutines SUB1 to SUB4, which are specialized to read the various data types instead of a single subroutine with many options. The material name MAT is read in the alphameric convention for KEDAK. The total cross section pointwise data are read and linearly interpolated for the group cross sections. In the actual status of the subroutine only smooth cross sections are treated correctly (like those of ${}^7\text{Li}$, for instance). Averaging with a weighting function must be introduced soon. Then elastic scattering is treated. The cross section is expected to be always available from KEDAK. The data are interpolated to get $\sigma_{el}(E_g)$, which in the Ii-notation is $\sigma_1(E_g)$. The angular distribution input data are read from KEDAK in the form of pointwise data, but the subroutine ANGIN is prepared to read also Legendre coefficients. It was not necessary, to make this option readily available. The subdivided points for the outgoing energy are transformed into scattering angles μ_c by the subroutine NARABE ("rearrangement"). We transcribe the interpolated (by INTER) angular distribution data to the energy array and integrate them over the subdivided energy points within ΔE_g with use of the subroutine XENER, to get the (unnormalized) kernel (i. e. angular distribution converted to E-space). To get $\sigma_1^0(g',g)$ we

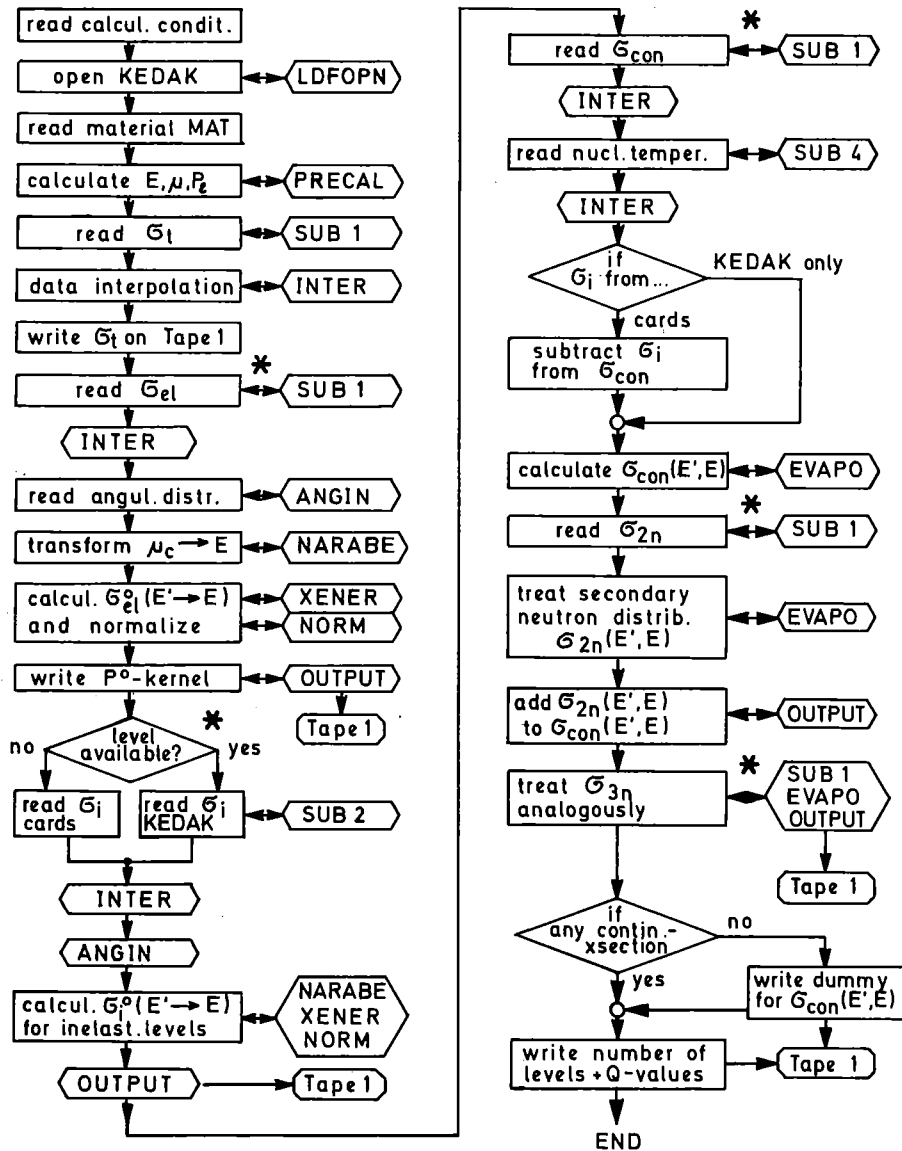


Fig. 13: Flow chart of NIO, simplified (* starting treatment of next reaction type)

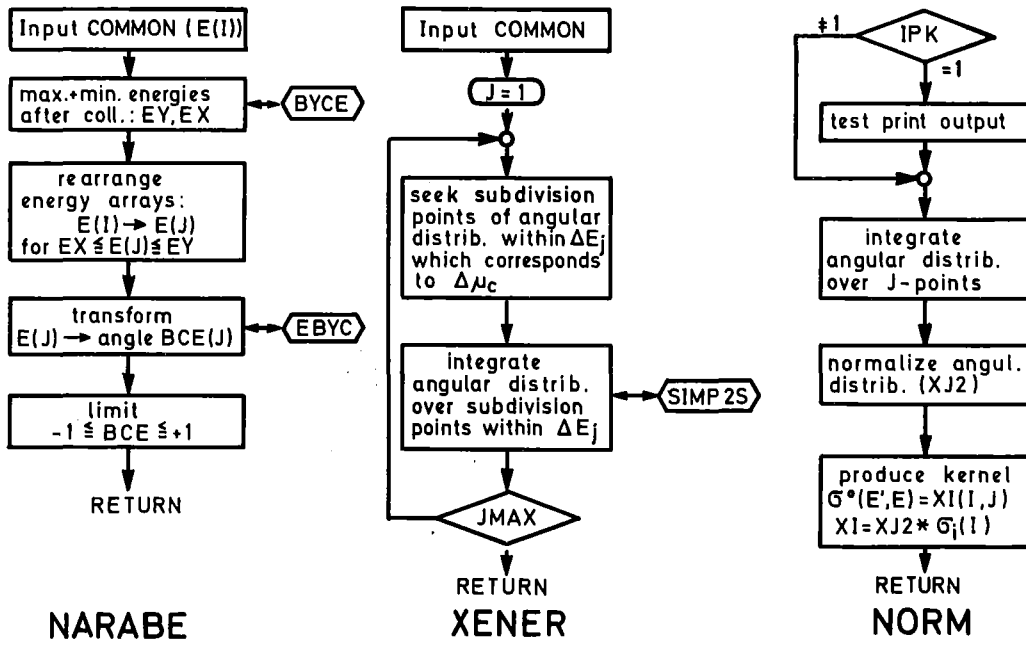


Fig. 14: Computational flow in three subroutines of NIO

integrate the unnormalized kernel within $E_{\min} \leq E_g \leq E_{\max}$, normalize the kernel to 1 and multiply then groupwise by $\sigma_1(E_{g'})$. This is done in subroutine NORM. This process is repeated for all groups of incident energy $E_{g'}$. The matrix $\sigma_1^0(g',g)$ is stored on tape No. 1 in the order of a sink group kernel (arrays in g' for fixed g).

For the level-inelastic scattering, the process can be repeated from the beginning at the cross section input, but just here technical changes are necessary, because the data input presents more problems. The program seeks at first for KEDAK data. If they are available, the further processing is done as for elastic scattering and the outgoing kernels are indexed with $i = 2, 3$, etc. If KEDAK data are not available, which is already true for the first attempt to read an angular distribution for the first level inelastic scattering, data can be read from cards. If a level cross section is read from cards in addition to KEDAK data, e. g. a second level cross section, where KEDAK contains only the first level cross section, this additional cross section(s) must be subtracted from the continuum cross section. This is done in NIO. For the inelastic scattering to the continuum the data table is read from KEDAK and interpolated to get $\sigma_{\text{con}}(g')$. Next we read the energy distribution of the secondary neutrons, actually only in the form of nuclear temperatures, as these data are given for the light elements (for Be not even this!). The subroutine EVAPO calculates $\sigma_{\text{con}}^0(g',g)$ by use of the formula

$$\sigma_{\text{con}}^0 = f_N \cdot \sigma_{\text{con}}(g') \cdot \frac{E_g}{T(g')^2} \cdot \exp\{-E_g/T(g')\} \quad (34)$$

with $E_g \leq E_{g'}$

with the normalization factor f_N :

$$f_N = 1 / \int_0^{E_{g'}} \frac{E_g}{T(g')^2} \cdot \exp \{-E_g / T(g')\} dE_g \quad (35)$$

The kernel $\sigma_{\text{con}}^0(g',g)$ is not immediately written on magnetic tape, because we must add to it the other possible continuum kernels, most probably the (n,2n) kernel.

The (n,2n) and (n,3n) kernels are treated in the same manner as the first continuum kernel, except for the normalization factor in EVAPO. These kernels, if existing, are added to the first continuum kernel and the final sum is written on tape No. 1, again in the form of a sink group kernel. It is this treatment of the nonelastic scattering, which we are least satisfied with. Improvements in this section are really necessary, e. g. evaluated double-differential data for the secondary neutrons. This point will be treated more extensively in section 5.

3.3.2 NIKER

The flow chart of NIKER is shown in Fig. 15. The continuation in NIKER for the calculational flow in the kernel production is demonstrated in Fig. 12. The flow chart of the most important subroutine of NIKER, FUNCII (for the Ii-function, resp. $T_i(n',n)$ matrix) is shown in Fig. 16. We start with the card input for the calculational conditions, including the μ_n set for the S_N calculation. The energy group boundaries and the total cross section are read from tape No. 1.

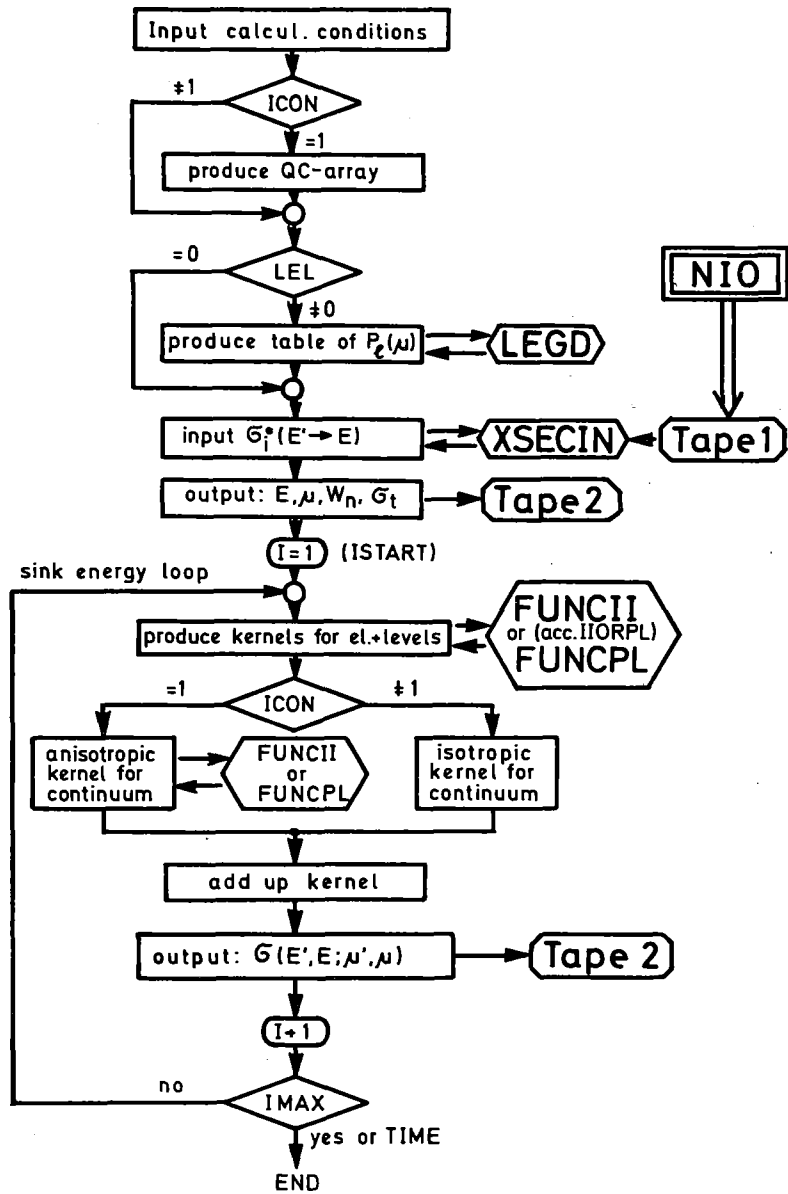


Fig. 15: Flow chart of NIKER

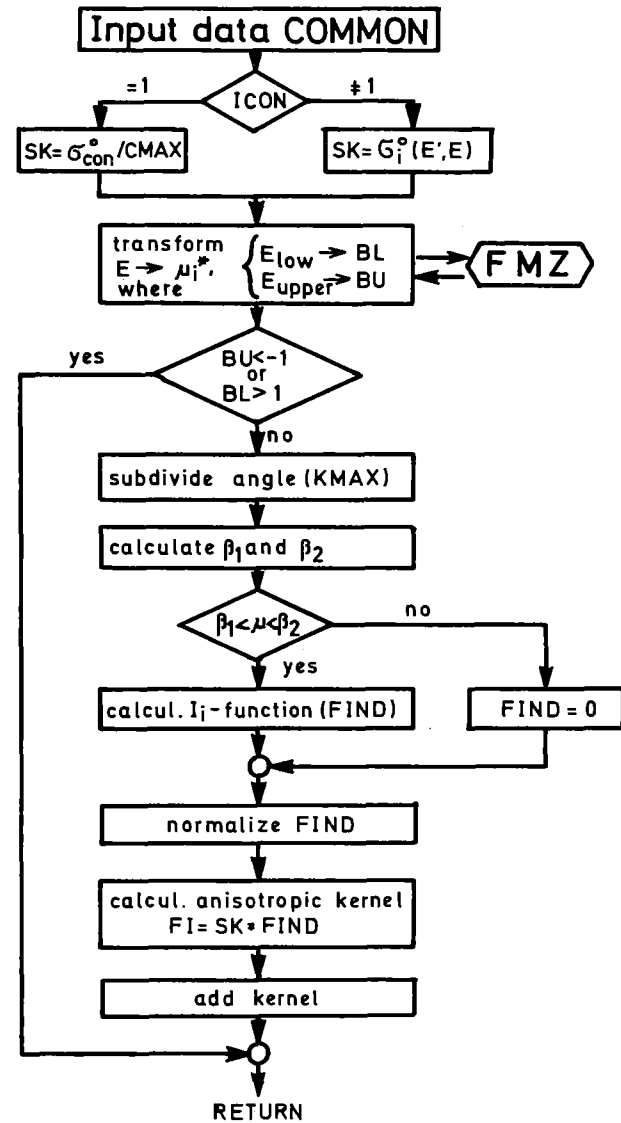


Fig. 16: Calculational flow in subroutine FUNCII of NIKER

NIKER has three options for generating anisotropic scattering matrices. With IIORPL = 1 the Ii-method is used. With IIORPL = 0 the P_L -method is used with a representation of the angular transfer probability in the entire range of μ - the usual method. With option IIORPL = -1 the P_L -function is set to zero outside the kinematically allowed range β_1 to β_2 , and renormalized inside this interval. Here we concentrate on the option for the Ii-method. The kernels are produced in a single sink group loop. Therefore the P_0 -kernels $\sigma_i^0(g',g)$, $i = 1$ to IL and $\sigma_{\text{con}}^0(g',g)$ are read from tape No. 1 at once.

Inside the sink energy loop the elastic and level-inelastic scattering is treated first by calling FUNCII with a specified Q_i -value and incident energy $E_{g'}$. In FUNCII (see Fig. 16) we calculate the cosine of the scattering angle, μ_i^* , in the LAB system, from $E_{g'}$, E_g and Q_i , based on Eq. (9) by means of the function subroutine FMZ. In Fig. 12 this is demonstrated as the step 3 to 4.

The outgoing energies within ΔE_g are subdivided into KMAX points. KMAX is defined automatically in the main routine of NIKER, such that the transformed angle points $\mu_i^*(g',g_K)$ give a slightly finer scale than the μ_n -set of the S_N -calculation. For instance, if we carry out a S_{32} calculation KMAX is set to somewhat more than 2 for ${}^7\text{Li}$, because - referring to the example of Fig. 12 - 22 energy groups correspond to the scattering from $-1 \leq \mu \leq 1$. Actually KMAX was set to at least 6 or 7, to keep the accuracy of the transformation. Next we calculate β_1 and β_2 for each μ_n , to restrict the μ_n -space. Then we calculate the angular transfer matrices $T_i(n',n)$ with Eq. (31) and average the obtained values over the KMAX points within $\Delta\mu_i^*$

that correspond to ΔE_g . The new matrix is called $T_i^*(n',n)$:

$$T_i^*(n',n) = \frac{1}{\Delta \mu_i^*} \cdot \sum_{g_k=1}^{KMAX} T_i(n',n) \cdot \Delta \mu_{g_k} \quad (36)$$

In order to keep the numerical accuracy we use the following normalization (normalize FIND in Fig. 16):

$$\sum_{n=1}^{NMAX} T_i^*(n',n) \cdot w_n = 1 \quad (37)$$

Then we get the anisotropic scattering matrix for scattering of type i:

$$G_i(g',g; n',n) = G_i^o(g',g) \cdot T_i^*(n',n) \quad (38)$$

In the first part of the sink energy loop this is done for the elastic and the level-inelastic scattering. The partial scattering matrices are added up into the FI-matrix, which finally contains:

$$G_{level}(g',g; n',n) = \sum_{i=1}^{IL} G_i(g',g; n',n) \quad (39)$$

Next in the sink energy loop we treat the kernel for the scattering to the continuum. The distribution of secondary neutrons is assumed as isotropic in the CM system. For a queue of assumed Q-values, which we call the Q_c -array and an element of it Q_{ci} , we transform the secondary energy distribution from the CM to the LAB system. According to Eqs. (32) and (33) the maximum and minimum energy for Q_{ci} is calculated and the section of the secondary neutron distribution between these limits is then treated as a P_o -kernel $\sigma_{ci}^o(g',g)$ in the same manner as the elastic and level inelastic kernels. In order to cover the entire distribution of secondary neutrons, the elements of the

Q_c -array are calculated such that the resulting E_{\max} and E_{\min} are overlapping by a certain portion, which is actually 30 %. This is shown in Fig. 17.

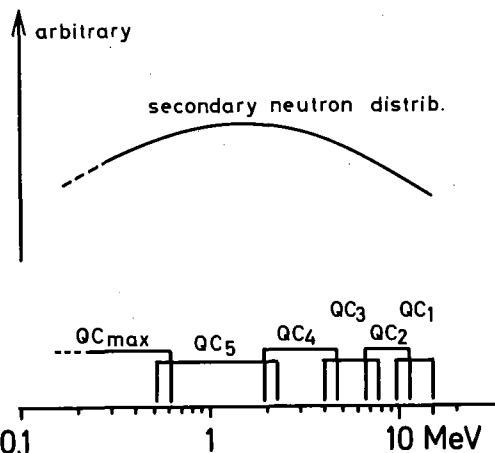


Fig. 17: Treatment of the c.m. to lab. transf. by means of assumed Q-values yielding overlapping energy intervals, here case of ${}^9\text{Be}$, 30% overlap. $QC_1=0$; and QC_{\max} for $E_{\min}(QC_{\max})=0$.

In this treatment we first assume the P_o -kernel $\sigma_{ci}^o(g',g)$ to be

$$\sigma_{ci}^o(g',g) = \sigma_{con}^o(g',g) / CMAX \quad (40)$$

where CMAX is the total number of the Q_{ci} . Then FUNCII is called to produce the angular transfer matrix $T_{ci}^*(n',n)$ to get

$$\sigma_{ci}(g',g; n',n) = \sigma_{ci}^o(g',g) \cdot T_{ci}^*(n',n). \quad (41)$$

This procedure is done for all Q_{ci} -values and the partial kernels are added and renormalized:

$$\sigma_{con}(g',g; n',n) = f_c \cdot \sum_{i=1}^{CMAX} \sigma_{ci}(g',g; n',n). \quad (42)$$

The normalization factor f_c is given by

$$f_c = \sigma_{con}^o(g',g) / \sum_{n=1}^{NMAX} \sum_{i=1}^{CMAX} \sigma_{ci}(g',g;n',n) \cdot W_n \quad (43)$$

Finally, we add the continuum kernel to the level-kernel to get the total anisotropic scattering kernel

$$\sigma(g',g;n',n) = \sigma_{level}(g',g;n',n) + \sigma_{con}(g',g;n',n). \quad (44)$$

This all being done for the sink energy group I, the results are stored on magnetic tape No. 2. The program returns to treat the kernels for the next sink energy group unless the last group has been reached or the computation time foreseen for the calculation has been consumed. For this case a continuation of the calculation in a subsequent job is foreseen, and ISTART is then the new starting group for the kernel calculation.

In the present stage of the development the continuum kernel is not added to the level kernel, but written separately on tape No. 2. At the expense of computer space the treatment became more straight-forward and allowed the control of errors and individual effects more effectively.

We have concentrated the work on light nuclei, because there we can demonstrate drastic effects, but some remarks must be made concerning heavier nuclei. For these the scattering - mainly elastic - is strongly peaked into the forward direction. If we use the energy group structure of table 1, the energy spread of the secondary neutrons covers only a small number of groups, e. g. 5 groups in the case of ^{56}Fe elastic scattering at 14.8 MeV incident neutron energy. As the angular distribution of secondary neutrons

in the CM system is converted to the P_0 -kernel $\sigma_i^0(g',g)$ by NIO, few groups must represent the anisotropy. This means, to stay with the above example of ^{56}Fe , that a S_{32} -calculation becomes effectively a S_5 -calculation only. In order to avoid such a decrease in accuracy, we could use a very fine energy group structure, but that makes the computations expensive. Another solution of this problem may be to restrict the use of a very fine energy group structure to NIO for the P_0 -kernel. In NIKER we then may come back to broader energy groups:

$$\sigma_g(g',g;n',n) = \sum_{i=1}^{IL} \frac{1}{\Delta E_g} \cdot \sum_{k=1}^{KMAX} \sigma_i^0(g',g_k) \cdot T_i(\mu_i^*(g_k); \mu_{n'}, \mu_n) \cdot \Delta E_{gk}$$

$$\text{with } E_{gk} = \Delta E_g - \frac{1}{2} \Delta E_g + k \cdot \Delta E_{gk}, \text{ and } \Delta E_{gk} = \Delta E_g / KMAX,$$

using the T_i probability of Eq. (31).

NIO and NIKER should be made able to carry out this procedure. However, if double differential cross section tables are given, we can avoid this procedure by using the Γ^* -method (see section 5.).

3.3.3 S_N -codes

We use the scattering matrices on tape No. 2 to calculate the neutron transport in a single isotope assembly. The flow chart of the one-dimensional code NITRAN-S for spherical geometry is shown in Fig. 18. It is a characteristic of the code that the scattering matrices are read inside the loop for the sink energy group. Moreover, it has an option to choose between two interpolation schemes to get the angular fluxes in a space-angle-cell, the linear or the exponential [24] scheme, steered with the input variable LORE. In the linear interpolation scheme we use

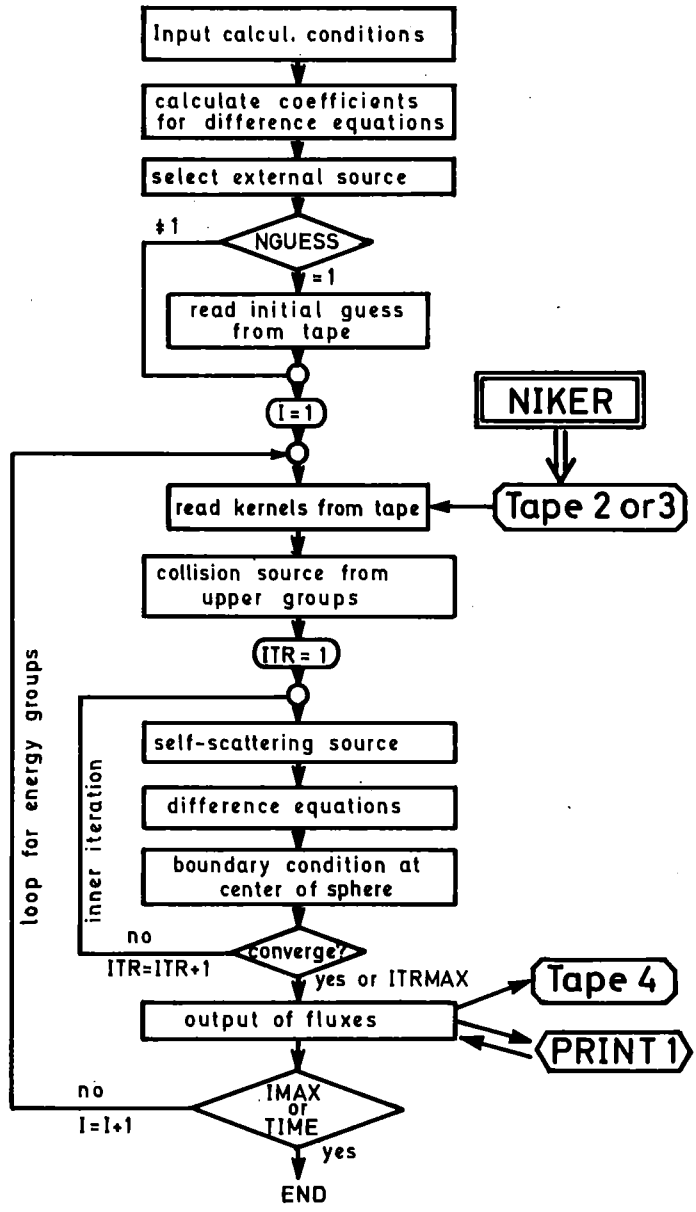


Fig. 18: Flow chart of NITRAN-S

$$F_g(m+\frac{1}{2}, n) + F_g(m-\frac{1}{2}, n) = 2 F_g(m, n) \quad (45)$$

$$F_g(m, n+\frac{1}{2}) + F_g(m, n-\frac{1}{2}) = 2 F_g(m, n) \quad (46)$$

with index g denoting the source group number, and the sink group being constant within the loop. For the exponential scheme [24] we use

$$F_g(m+\frac{1}{2}, n) \cdot F_g(m-\frac{1}{2}, n) = F_g(m, n)^2 \quad (47)$$

$$F_g(m, n+\frac{1}{2}) \cdot F_g(m, n-\frac{1}{2}) = F_g(m, n)^2 \quad (48)$$

At the centre of the sphere, where we have

$$F_g(\frac{1}{2}, \mu) = F_g(\frac{1}{2}, -\mu) \quad (49)$$

as the boundary condition, we use a linear interpolation in μ , which makes it possible to use an unsymmetric set of angular mesh points, μ_n .

An unsymmetric μ_n set is useful for fusion neutronics applications, because densely distributed μ -points in the forward direction are needed to allow for the good description of the strong forward anisotropy of the neutron flux [14].

NITRAN-S has three options for negative flux correction, steered by the input variable NFC. If we use negative flux fix-up, unnegligible errors will be produced. To correct for these, rebalancing of neutrons has to be used. Up to now, it was unnecessary to introduce this rebalancing for the following reasons. When applying the I_i -method it is only by the linear interpolation

scheme and by numerical effects in the computer that negative fluxes are produced. Their absolute values, however, are small. Moreover, the microscopic neutron balance [19] is sustained by the difference equation itself, because the collision source term is rigorously treated by the Ii-method and we use a sufficiently fine spatial mesh width. A test calculation for a vacuum sphere with a spherical shell source gave a result which was very close to an analytically obtained result. For a calculation also without rebalancing, but with negative flux correction, the result differed by several percent from the others. The exponential method, as proposed in ref. [24], was introduced into NITRAN-S to allow for larger spatial mesh widths without losing accuracy. In ref. [24] it was stated, that the problems of the negative flux generation is not solved by this interpolation method alone, but that a non-negative collision source term formulation is also necessary (see Fig. 3). The Ii-method therefore should be used in conjunction with the exponential scheme. Unfortunately, we failed to make successful calculations, when using the equations given in ref. [24]. Perhaps they contain some error. But in view of the promises of this interpolation scheme we will continue the efforts to use it.

In this report, we present only results of calculations without negative flux correction.

The inner iteration is stopped in the usual way, the changes are printed for control. The outer iteration is not yet needed, therefore the results can be written group by group on magnetic tape No. 4 after the end of each inner iteration (there is no up-scattering).

4. Test calculations and results

4.1 Testing the accuracy of the P_L -method and comparing the calculational speeds

4.1.1 Calculational conditions

NIKER has an option to produce anisotropic scattering matrices based on Eqs. (15) to (19), i. e. according to the P_L -method (input variable IIORPL = 0).

Using this option four P_L -kernels were produced for ${}^7\text{Li}$: P_1 , P_3 , P_5 and P_{20} . The reference kernel was produced by the Ii-method (IIORPL = 1). The comparison concerns elastic scattering only, non-elastic scattering treatment was unchanged. The input data were for elastic scattering ENDF/B-IV, processed by SUPERTOG [8], for non-elastic a collection of data from ENDF/B-IV, ENDL and BNL 400, processed by NIO. These are described in section 4.2, where they are more relevant than here. In NIKER they were treated as isotropic in the LAB system. Only the elastic scattering was treated with the full anisotropy in both the CM and the LAB system.

S_{32} -calculations with NITRAN-S, using the μ_n -set of table 2*) were carried out for a sphere of ${}^7\text{Li}$ with 50 cm radius and 1 cm radial mesh width. The D-T-source was located at a central shell of 2 cm radius, and the measured spectrum of the source in the lithium sphere experiment [14] was used. 67 energy groups (see table 1*) were used for all calculations.

4.1.2 Results for flux and reaction rate

As had been expected the higher order P_L -calculations yield results for reaction rates so close to the reference Ii-calculation, that we present the

*) At the end of the paper

relative deviation from the reference at an expanded scale in Fig. 19. The rate calculation with the P_5 approximation is already so close to the reference values that we omitted the P_{20} result.

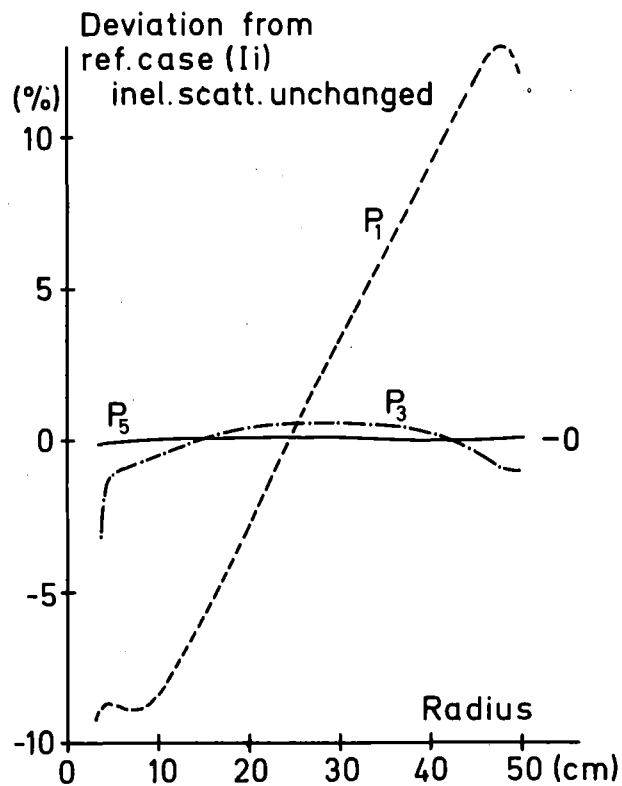


Fig. 19: ${}^7\text{Li}$ -sphere, accuracy of P_L method with respect to calc. of T-rate

Here it must be pointed out again, that the above comparison between the P_L - and the Ii-method concerns the elastic scattering only, and that one cannot draw conclusions on the accuracy of the entire calculations.

In the rate calculation we have a lot of error compensation. The situation with the fluxes, especially the angular fluxes, is already much worse, as can be seen from Fig. 20.

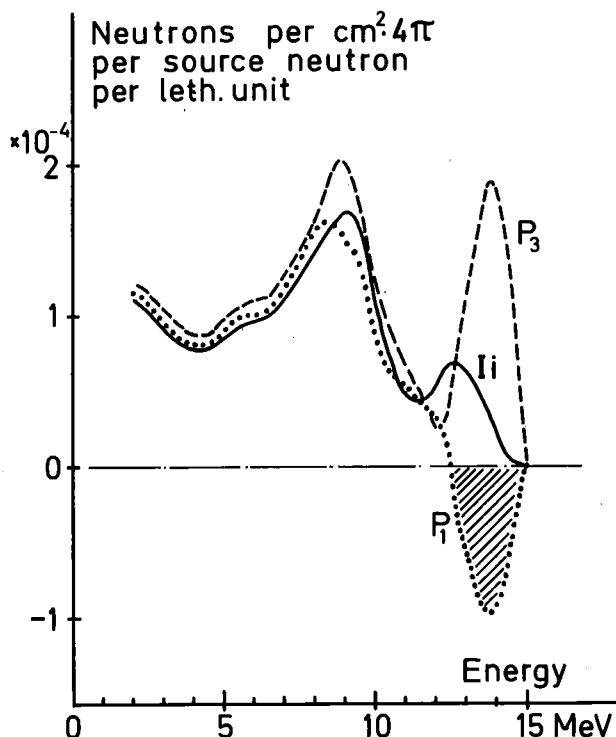


Fig. 20: ${}^7\text{Li}$ -sphere: calc. angular flux at $r=10.5\text{cm}, 93^\circ$; various methods for elastic scattering

In P_L -calculations of low order large discrepancies are found in the energy region, where we have most probably neutrons with single interactions. These errors propagate spatially and energetically. After several interactions the randomization of the errors provides a compensation. In fact, below 10 MeV the P_5 -results - and of course the P_{20} results, too - were so close to the reference, that we did not include them into Fig. 20. However, P_5 -calculations and even P_{20} -calculations give rise to serious problems with negative fluxes in the backward directions [12, 13]. We expect the error compensation to work less effectively in the neighbourhood of a major local heterogeneity like a duct or a strongly absorbing rod.

From this point of view a rigorous reference method is needed to allow an estimate of the errors also for those more complicated geometries. Therefore, also a two-, or even three-dimensional S_N -code should be developed, which uses the Ii-method.

4.1.3 Computational speed of the Ii-method

In the NITRAN system the computation time needed for a S_N -calculation is independent from the scattering kernel calculations. Therefore, the computation time for the Ii-method can be compared with that for the P_L -method by comparing the time needed to compute the scattering matrices with NIKER. For the P_L -method, this depends on the order L . Naively and from the general experience with rigorous reference methods one expects a statement like the following: "In view of the rigorous reference results the calculational speed is still acceptable." However, as Fig. 21 shows, the calculational speed of the Ii-method lies between that of P_3 - and P_5 -calculations. Therefore the Ii-method is not only suited for accurate reference calculations, but also for practical use in technical calculations.

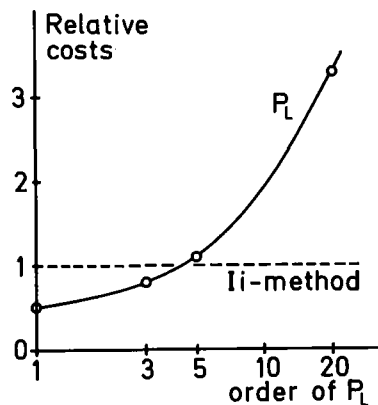


Fig. 21: Relative costs of collision source calculations with NIKER

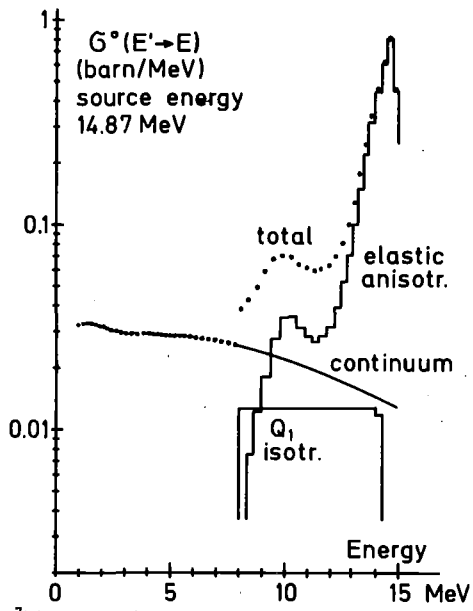
4.2 Effect of the anisotropy of the non-elastic scattering

4.2.1 In ^7Li , referring to the lithium sphere experiment [14]

In order to show the effect of the anisotropy of the non-elastic scattering, we had to prepare two scattering matrices, which were identical for the elastic part. These elastic data were - as in section 4.1 - taken from ENDF/B-IV, processed by SUPERTOG [8]. The program NIKER treated these data by the Ii-method, taking into account the full anisotropy in the CM and the LAB system.

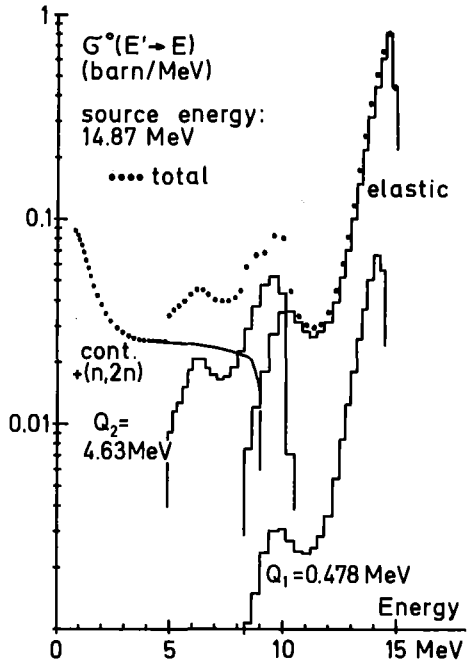
The first kernel contained the non-elastic scattering in fully isotropic form, i. e. the secondary neutrons were assumed to be isotropic in both the CM and the LAB system. Input data were taken from KEDAK [23], which were transcribed data from ENDF/B-III. These data consist of the first level inelastic scattering cross section, the continuum cross section and the (n,2n) cross section. The secondary neutron distribution for the latter two is given by nuclear temperatures. An example of the intermediate kernel $\sigma^0(g',g)$, the input to NIKER, is shown in Fig. 22a.

The second kernel contained the nonelastic scattering as far as possible in fully anisotropic form. Data were taken mainly from ENDF/B-IV. As this data set includes only the first level cross section, the data for the second level cross section were taken from ENDL [25] and some data for the angular distribution from BNL 400 [26]. The second level cross section was, of course, subtracted from the continuum cross section. For the angular



⁷Li secondary neutron distributions
 elastic: ENDF/B-4
 inelastic: ENDF/B-III (KEDAK)

Fig. 22 a:



⁷Li: secondary neutron distribution,
 anisotropic data: ENDF/B-4+ENDL+BNL400

Fig. 22 b:

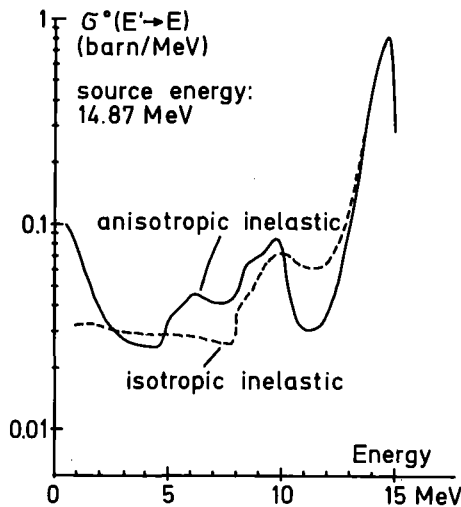


Fig. 22 c: ⁷Li: secondary neutron distributions,
 anisotr. data: ENDF/B-4+ENDL+BNL400,
 isotr. data: KEDAK (1inel. level only)

distribution of the first level inelastic scattering the data of the elastic scattering were taken. This approximation is allowed in view of the fact that the Q-value (.478 MeV) is low compared with the incident neutron energy 14 MeV. Thus an estimate of the anisotropy in the CM system is included in the data set, which then was treated by the NIKER code with the Ii-method. In Fig. 22 b an example of the intermediate kernel for this case is shown. In Fig. 22 c the total secondary neutron distributions for both cases are compared. The second kernel has remarkably less high-energy neutrons.

For the anisotropic case in NIKER the continuum inelastic and (n,2n) scattering was treated by use of assumed Q-values (see section 3.3.2). Both neutrons of the (n,2n) process were treated by inelastic scattering kinematics to produce the anisotropy in the LAB system. This is not fully correct, but the contribution of (n,2n) to the total continuum scattering is small for ${}^7\text{Li}$.

Due to all the approximations for the anisotropic kernel the data set serves only for the demonstration of the effect of the anisotropy of the non-elastic scattering on neutron transport. The S_{32} -calculations with NITRAN-S were done in the same way as in section 4.1, the only difference being the scattering kernels. Fig. 23 presents calculated scalar flux spectra for both cases. Ratios of scalar fluxes are shown in Fig. 24 a and b. These figures show that the scalar fluxes in average in the sphere are overestimated by as much as 35% (except for the source energy region) unless we include the anisotropy of the non-elastic scattering. The effect

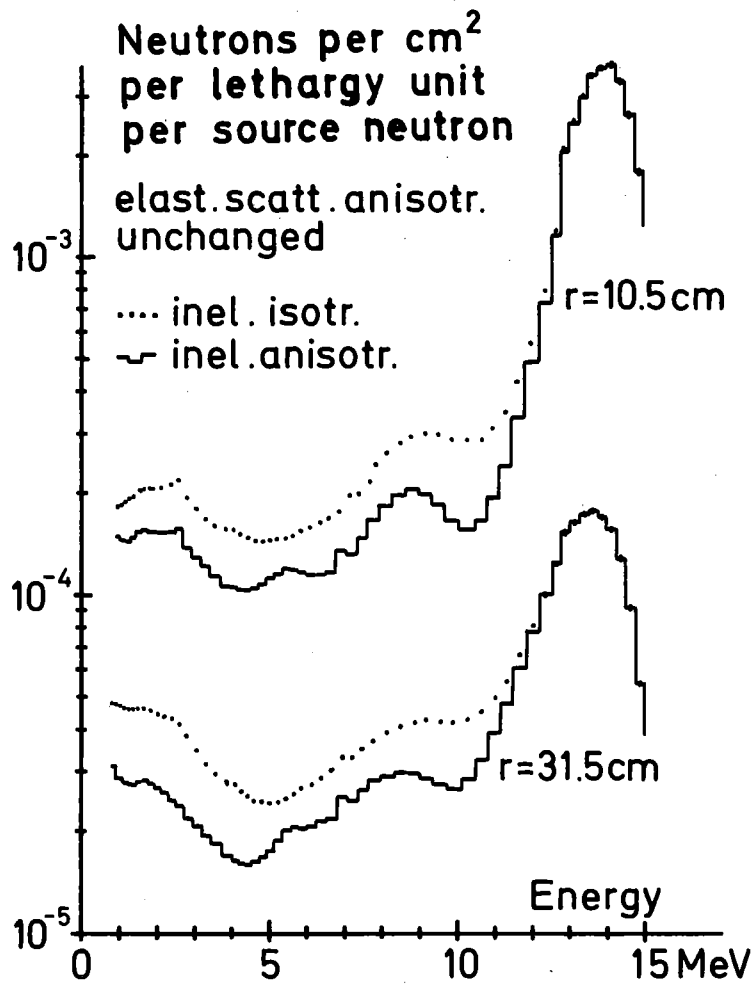
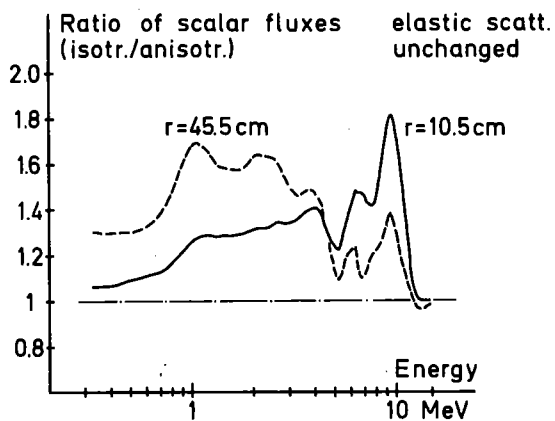


Fig. 23: ⁷Li-sphere: effect of inel. scattering anisotropy on scalar spectra, anisotr. calcul. by li-method, S₃₂



⁷Li-sphere, local effect of inel. anisotropy

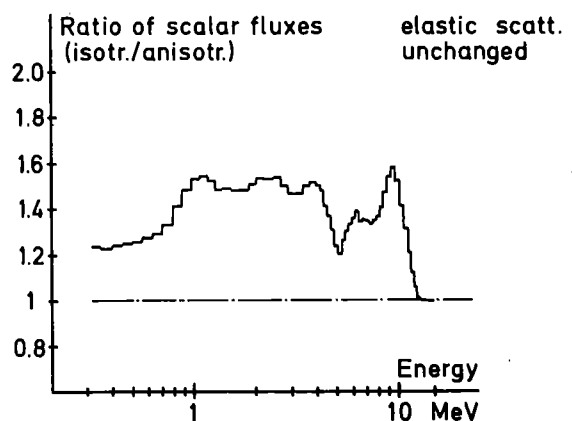


Fig. 24 b:

Fig. 24 a:

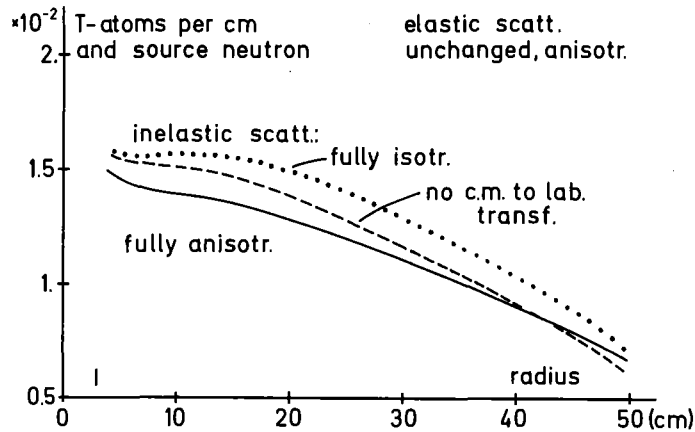


Fig. 25: ⁷Li-sphere, calculated tritium production rate

Table 3

		Tritium breeding isotope		
		⁷ Li	⁶ Li	⁷ Li+ ⁶ Li
NITRAN	isotr. inel.	0.598*	(0.115)*	0.713*
S ₃₂ -Ii	anisotr. inel.	0.526*	(0.080)*	0.606*
DTK	isotr. inel.	0.569	0.115	0.684
S ₁₉ -T ₅				
Experiment	KfK	-	-	0.43 ± 0.035

Comparison of calculated and measured tritium breeding ratios for a lithium metal sphere of 1m diam., measured source spectrum in calcul. *: from flux in pure ⁷Li

depends on the distance from the source. The effect is large in the higher energy region for positions near the source. More distant from the source, where the lower-energy neutrons are produced by subsequent collisions after a first interaction at higher energy, it propagates to lower energies. The effect for the scalar fluxes integrated over the whole sphere is naturally dependent on the size of the sphere: If we calculate the fluxes in a very large assembly, the effect appears only according to the energy dependence of the spectrum and the reaction cross section.

Fig. 25 presents calculated tritium production rates by the ${}^7\text{Li} (n, n'\alpha)\text{T}$ reaction for the calculations with the two kernels. The effect of the anisotropy of the non-elastic scattering is about 15% in average and up to 18% near the source. A third, dashed curve in Fig. 25 is the result of a calculation with a kernel in which the anisotropy of the non-elastic scattering was taken into account for the CM system, but the CM to LAB system transformation not being performed. Thus, it can be seen that the major part of the effect is due to the anisotropy of the scattering in the CM system.

In Table 3 the tritium breeding ratios, i. e. the tritium production rate integrated over the sphere, are listed for the various calculations as well as the results of the Karlsruhe lithium sphere experiment [14]. This experiment was carried out with natural lithium in a spherical container of stainless steel. In view of the low content of ${}^6\text{Li}$ (7.42%) in natural lithium and the very similar elastic scattering we

can approximate the natural lithium by pure ^7Li for the neutron transport calculation. Moreover, since the treatment of the neutron transport in the target support can be eliminated by using the measured spectrum of the target support [14], we were able to simplify the problem to a transport calculation in a single material zone with a single isotope. The results for the calculation with isotropic non-elastic scattering are not perfectly identical, because there are differences in the calculational methods and slightly different data for elastic scattering were used.

The relative change of the tritium breeding ratio due to the inclusion of the anisotropy of the non-elastic scattering is 18%. Fig. 26 shows two angular spectra of ref. [14], together with spectra calculated with NITRAN-S for pure ^7Li , as described before. This figure is to be compared with Fig. 5, in which the calculated spectra do not include the anisotropy of the non-elastic scattering. The large discrepancy in Fig. 5 between measured and calculated spectra is seen to be greatly reduced. The shift of the elastic and the second level inelastic peak is due to the isotropic source spectrum, which does not take into account the kinematics of the D-T-reaction. In ref. [14] an effect of 13 to 20% on the tritium production rate was derived from the observed discrepancy between measured and calculated angular spectra. The then suggested origin of that discrepancy, namely the anisotropy of the non-elastic scattering not being included in the calculation, is confirmed by our present investigation (18% at about $r = 10$ cm). Having included a first estimate of the anisotropy of the non-elastic scattering there remain errors, which can be attributed to a manifold of origins, except for the method to calculate the collision source

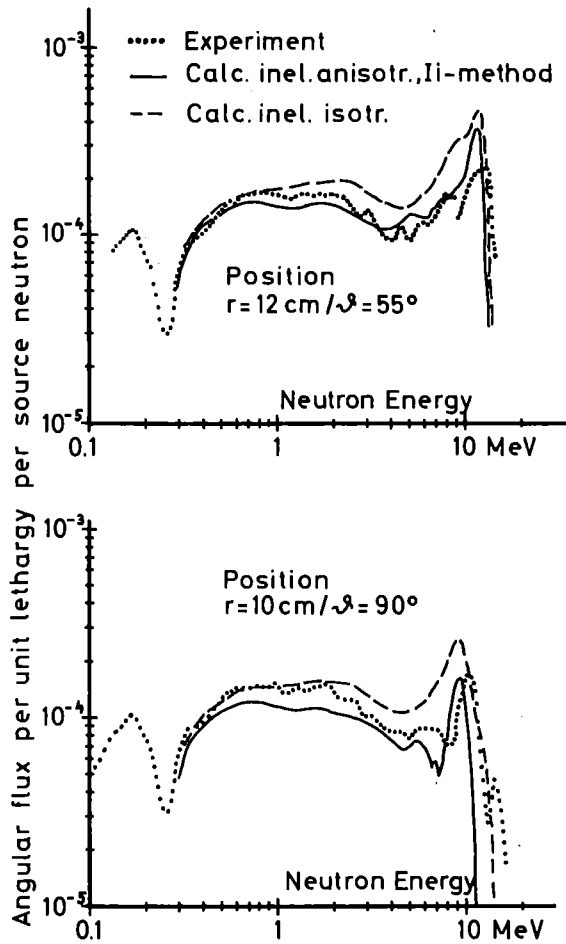


Fig. 26: Li sphere: comparison of measured and calc. angular spectra. Calculation pure ${}^7\text{Li}$, meas. source spectrum, elast. scatt. by Ii method.

term. Besides the error of replacing the ${}^6\text{Li}$ by ${}^7\text{Li}$ in the above calculation we list some further sources of errors, in a crude order of presumed importance.

- a) The ${}^7\text{Li}$ (n,n' α) T total cross section value at 14 MeV may be too high. This is the main reason for the rest of the discrepancy in the tritium breeding ratio [14].
- b) Angular distribution of elastic scattering at 14 MeV seems to be incorrect at 55° ($\hat{=} \mu = 0.574$), see Fig. 26 at the high energy peak.
- c) Angular distribution of secondary neutrons not taken into account for continuum-non-elastic, which includes the (n,n' α) and the (n,2n) reaction.

4.2.2 Effect in spheres of ${}^9\text{Be}$ and ${}^{12}\text{C}$

In the actual KEDAK data for ${}^9\text{Be}$ there is no information on the angle- or energy-distribution of secondary neutrons from the (n,2n) reaction. Therefore we produced scattering matrices by assuming the evaporation model with nuclear temperatures lent from the ${}^7\text{Li}$ (n,n' α) data. This enables us to give a rough estimate of the effect of the CM- to-LAB system transformation by using the kinematics of inelastic scattering for both neutrons (see section 3.3.2). In Fig. 27, a and b, the effect of the CM to LAB system transformation is shown for a Be-sphere of 20 cm radius.

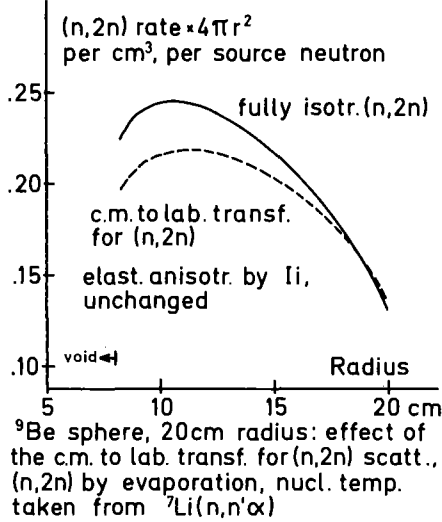


Fig. 27 a:

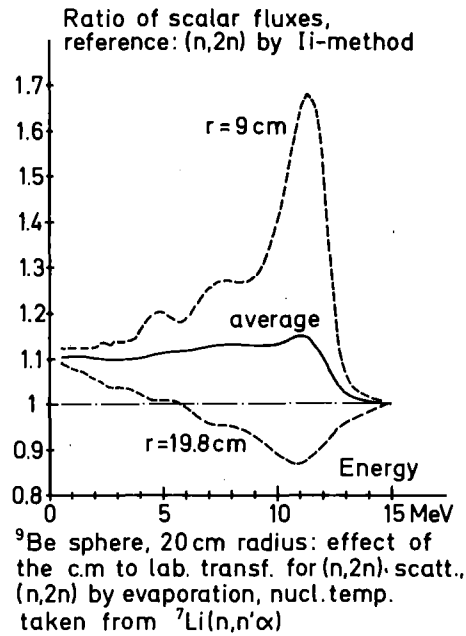


Fig. 27 b:

A fraction of the "first neutron" from ⁹Be (n,2n) comes from inelastic level scattering. Recent works on the secondary neutron distributions from scattering on ⁹Be [27, 28] show that in ENDF/B-IV this fraction on inelastic level scattering is overestimated. Consequently, as the (n,2n) cross section is agreeing with the newer measurements, the contribution of reaction channels as ⁹Be (n, α) ⁶He* and the direct multiparticle breakup, which provide neutrons of lower energies, are underestimated. When calculating the multiplication effect of a beryllium layer with ENDF/B-IV data there are three sources of errors, which all increase the estimate of the effect. Firstly, an increased fraction of higher-energy neutrons allows more second (n,2n) interactions after a first one. Secondly, neglecting the anisotropy of the non-elastic scattering increases the scalar fluxes near the source, and thirdly, omitting the CM to LAB system transformation affects the calculation in the same way. Thus, we can understand that there is a great discrepancy between the measured and calculated multiplication factor of a beryllium layer in ref. [4]. Moreover, for the fusion reactor

design of ref. [29], in which the molten salt Li_2BeF_4 ("Flibe") is proposed, and for which a tritium breeding ratio of 1.07 has been calculated, it is to be feared that the breeding is less than marginal, even if the reserves of the design are exhausted.

For ^{12}C the inelastic scattering is given in KEDAK as 5 level scattering cross sections in contrast to ENDF/B-IV. But no information on angular distributions of the secondary neutrons, except for the elastic scattering, is given. Therefore, as for ^9Be , we can only present the effect of the CM- to-LAB system transformation.

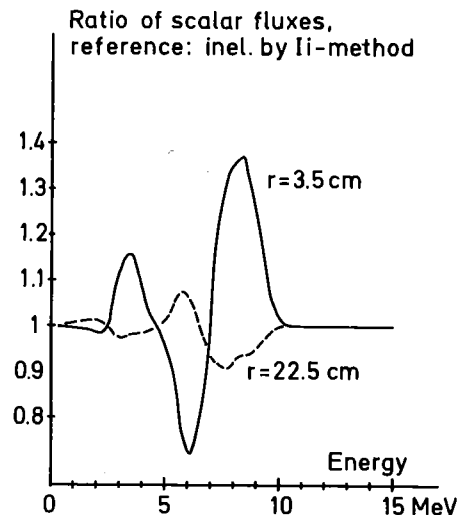


Fig. 28: ^{12}C sphere, 23cm radius: effect of the c.m. to lab. transf. for inel. scattering. data KEDAK: inel. levels up to 14 MeV, isotropic in c.m.s.

This effect is shown in Fig. 28 referring to the scalar fluxes. The effect is large, even for the mass of 12. There are few data available [26] for angular distributions from level scattering on the Q_1 , Q_2 and Q_3 levels. These data indicate that they should not be neglected [12].

5. The I*-method

5.1 Double differential cross section

In the present NITRAN-system we need both the reaction cross section and angular (or energy) distribution data (single differential cross section with respect to outgoing angle or energy). We also need the collision kinematics in order to reconstruct the complete scattering kernel. Therefore we need a large amount of detailed nuclear data for every reaction in every isotope to calculate the neutron transport accurately. This situation originates from the strategy of nuclear data compilation and evaluation in the existing nuclear data files: we have normalized angular distributions of secondary neutrons for various reactions, and there are some other reactions, for which the secondary energy distributions are given. For lower energies, up to several MeV, this strategy is quite useful, but above that the work to reconstruct the full scattering kernel increases with the number of reaction channels. This makes the data processing in NIO and NIKER complicated. Besides the rise in efforts due to the data storage in partial cross sections there is the problem of missing information, so that the scattering kernel cannot be reconstructed completely, as was the case for all our examples in the preceding section.

If the double differential neutron emission cross section in the LAB system, $\sigma(E', E; \mu_0) = 2\pi \cdot \frac{\partial^2 \sigma}{\partial \Omega_0 \partial E}$, were given in an evaluated nuclear data file for each material (or isotope, if needed in this form), the data processing for the scattering kernel calculation would become very simple. The transport calculations following the Ii-method must then be modified. The modified

Ii-method is shown to be an independent rigorous method, and therefore it is called the I*-method.

In the Ii-method (see section 2.) double differential cross sections are related to their data processing by the following formulae, which use single differential cross sections with respect to the scattering angle:

$$\left(\frac{\partial^2 \sigma}{\partial \Omega_0 \partial E} \right)_{\text{aniso}} \equiv \frac{1}{2\pi} \sigma(E', E; \mu_0) \quad (50)$$

$$= \frac{1}{2\pi} \sum_{i=1}^{IL} \left(\frac{\partial \sigma_i}{\partial \mu_0} \right) \cdot \left(\frac{\partial \mu_0}{\partial E} \right) \cdot \delta(\mu_0 - \mu_i^*) \quad (51)$$

$$= \frac{1}{2\pi} \sum_{i=1}^{IL} \sigma_i(E', \mu_0) \cdot \left(\frac{\partial \mu_0}{\partial E} \right) \cdot \delta(\mu_0 - \mu_i^*) \quad (52)$$

$$= \frac{1}{2\pi} \sum_{i=1}^{IL} \sigma_i(E', \mu_c) \cdot g_i(E') \cdot \delta(\mu_0 - \mu_i^*), \quad (53)$$

where μ_i^* is dependent on the kinematics of the collision type i , and

$$\left(\frac{\partial^2 \sigma}{\partial \Omega_0 \partial E} \right)_{\text{iso}} \equiv \frac{1}{4\pi} \sigma_{\text{iso}}(E', E). \quad (54)$$

where μ_0 and μ_c express the scattering angles for the LAB and the CM system, respectively, with $\frac{\partial \sigma_i}{\partial \mu_0} \equiv \sigma_i(E', \mu_0)$. In the I*-method we start from the double differential cross section, which no longer needs the information on the collision type. We use the next formula as an operator in the I*-method.

$$\frac{\partial^2 \sigma}{\partial \Omega_0 \partial E} \equiv \int_{-1}^{+1} \frac{\partial^2 \sigma}{\partial \Omega_0 \partial E} \cdot \delta(\mu_0 - \mu^*) d\mu^* \equiv \frac{1}{2\pi} \int_{-1}^{+1} \sigma(E', E; \mu^*) \delta(\mu_0 - \mu^*) d\mu^* \quad (55)$$

This angular transformation operator is based on the idea that the cosine

of the angle between the incident neutron vector $\vec{\Omega}'$ and the outgoing neutron vector $\vec{\Omega}$ is identical to the cosine of the scattering angle, which is given as parameter of the double differential cross section.

The operator works as:

$$G(E', E; \mu_0) f_g(\vec{r}, \mu', \varphi') = \int_{-1}^{+1} G(E', E; \mu^*) \delta(\mu_0 - \mu^*) f_g(\vec{r}, \mu', \varphi') d\mu^* \quad (56)$$

It is the purpose of the I^* -method to reduce the number of angular variables to the only meaningful one, i. e. the scattering angle μ^* . This is the origin of the high calculational speed of this method (and the I -method, but there it is not so obvious). This has not been recognized in ref. /34/.

5.2 The neutron balance equation and its collision source

The neutron balance equation for the angular flux $f_g(\vec{r}, \vec{\Omega})$ in an energy group g is expressed by

$$\begin{aligned} \vec{\Omega} \cdot \vec{\nabla} f_g(\vec{r}, \vec{\Omega}) + G_t^g f_g(\vec{r}, \vec{\Omega}) &= \\ &= \frac{1}{2\pi} \sum_{g'} \int_{-1}^{+1} \int_0^{2\pi} G(g', g; \mu_0) f_{g'}(\vec{r}, \mu', \varphi') d\varphi' d\mu' + \\ &+ \frac{1}{4\pi} \sum_{g'} G_{i,so}(g', g) \int_{-1}^{+1} \int_0^{2\pi} f_{g'}(\vec{r}, \mu', \varphi') d\varphi' d\mu' + S_g(\vec{r}, \vec{\Omega}) \end{aligned} \quad (57)$$

where the energy variables are already discretized and

$$\mu_0 \equiv \vec{\Omega}' \cdot \vec{\Omega} = \mu\mu' + \sqrt{1-\mu^2} \cdot \sqrt{1-\mu'^2} \cos(\varphi' - \varphi). \quad (58)$$

We may combine $\sigma(g',g;\mu_0)$ and $\sigma_{iso}(g',g)$ to get a single kernel, however we keep the two separately, because the anisotropic treatment is not always needed, particularly for the lower energy region. By using Eq. (56) we rewrite the anisotropic collision source term as:

$$\begin{aligned} (\text{coll. source})^{aniso} &= \\ &= \frac{1}{2\pi} \sum_{g'} \int_{-1}^{+1} \int_0^{2\pi} \int_{-1}^{+1} \sigma(g',g;\mu^*) \delta(\mu_0 - \mu^*) \cdot f_{g'}(\vec{T}, \mu', \varphi') d\mu^* d\varphi' d\mu' \end{aligned} \quad (59)$$

At first we perform the integration over φ' , following the same path as described in Appendix 1, and obtain:

$$\begin{aligned} (\text{coll. source})^{aniso} &= \\ &= \sum_{g'} \int_{-1}^{+1} \int_{\beta_1^*}^{\beta_2^*} \sigma(g',g;\mu^*) \cdot I^*(\mu^*; \mu', \mu) \cdot f_{g'}(\vec{T}, \mu', \varphi + \Delta^*) d\mu^* d\mu' \end{aligned} \quad (60)$$

where the phase shift Δ^* in the φ -space is

$$\Delta^* = \arccos \left(\frac{\mu^* - \mu\mu'}{\sqrt{1-\mu^2} \cdot \sqrt{1-\mu'^2}} \right) \quad (61)$$

For fixed μ' and μ there is a restricted range of the scattering angle

$\mu^* : \beta_1^* < \mu^* < \beta_2^*$, where

$$\beta_1^* = \mu\mu' - \sqrt{1-\mu^2} \sqrt{1-\mu'^2} \quad (62)$$

$$\beta_2^* = \mu\mu' + \sqrt{1-\mu^2} \sqrt{1-\mu'^2} \quad (63)$$

The angular transfer probability function $I^*(\mu^*; \mu', \mu)$ is given by the same equation as the Ii-function (Eq.(10)), but here we use μ^* as an independent variable in the collision kinematics.

$$I^*(\mu^*; \mu', \mu) = \frac{1}{\pi \sqrt{1-\mu^2 - \mu'^2 - \mu^{*2} + 2\mu\mu'\mu^*}} \quad \text{for } \beta_1^* < \mu^* < \beta_2^* \quad (64)$$

$$= 0 \quad \text{for } \mu^* \leq \beta_1^* \quad \text{or} \quad \mu^* \geq \beta_2^* .$$

Of course, the I^* -function has the same characteristics as the I -function, and in the same way as for the I -function we can show that the I^* -method corresponds to the P_L -method with $L \rightarrow \infty$. The neutron balance equation (Eq. (57)) is rewritten as:

$$\begin{aligned} \vec{\Omega} \cdot \vec{\nabla} f_g(\vec{r}, \vec{\Omega}) + \Sigma_t f_g(\vec{r}, \vec{\Omega}) &= \\ &= \sum_{g'} \int_{-1}^{+1} \int_{\beta_1^*}^{\beta_2^*} \Sigma(g', g; \mu^*) \cdot I^*(\mu^*; \mu', \mu) \cdot f_{g'}(\vec{r}, \mu', \varphi + \Delta^*) d\mu^* d\mu' + \\ &+ \frac{1}{4\pi} \sum_{g'} \Sigma_{iso}(g', g) \Phi_{g'}(\vec{r}) + S_g(\vec{r}, \vec{\Omega}) \end{aligned} \quad (65)$$

where $S_g(\vec{r}, \vec{\Omega})$ is the external source, and the definition of the scalar flux is

$$\Phi_g(\vec{r}) \equiv \int_{-1}^{+1} \int_0^{2\pi} f_g(\vec{r}, \vec{\Omega}) d\varphi d\mu \quad (66)$$

In the I^* -method we integrate over μ^* . Another approach to the use of double differential cross sections, in which the collision source is calculated by integrating over $\vec{\Omega}$, is discussed later.

We have to treat the phase shift Δ^* to solve the transport equation, except for the case of the one-dimensional calculation, where we bypass the Δ^* -treatment. For a spherical assembly the balance equation becomes in the I^* -formulation:

$$\begin{aligned}
 & \frac{\mu}{r^2} \frac{\partial}{\partial r} [r^2 F_g(r, \mu)] + \frac{1}{r} \frac{\partial}{\partial \mu} [(1-\mu^2) F_g(r, \mu) + G_c^* F_g(r, \mu)] = \\
 & = \sum_{g'} \int_{-1}^{+1} \left[\int_{\beta_1^*}^{\beta_2^*} G(g', g; \mu^*) \cdot I^*(\mu^*; \mu', \mu) d\mu^* \right] \cdot F_{g'}(r, \mu') d\mu' + \\
 & + \frac{1}{2} \sum_{g'} G_{iso}(g', g) \int_{-1}^{+1} F_{g'}(r, \mu') d\mu' + S_g(r, \mu) .
 \end{aligned} \tag{67}$$

5.3 Relation between the I^* - and the Ii-method

In the Ii-method the anisotropic scattering kernel of the transport equation is related to

$$K(E', E; \mu', \mu) \equiv \int_0^{2\pi} \left(\frac{\partial^2 G}{\partial \Omega_0 \partial E} \right)_{aniso} d\Delta \tag{68}$$

$$= \frac{1}{2\pi} \sum_{i=1}^{iL} \int_0^{2\pi} G_i(E', \mu_c) g_i(E') \delta(\mu_0 - \mu_i^*) d\Delta . \tag{69}$$

where $\Delta = \varphi' - \varphi$. From the knowledge in Appendix I the kernel is expressed by means of the Ii-function:

$$K(E', E; \mu', \mu) = \sum_{i=1}^{iL} G_i(E', \mu_{ci}^*) g_i(E') \cdot \bar{I}_i(\mu', \mu) . \tag{70}$$

In an analogous way the kernel is derived for the representation by means of the I^* -function using Eq. (55):

$$K(E', E; \mu', \mu) = \int_{-1}^{+1} G(E', E; \mu^*) \int_0^{2\pi} \delta(\mu_0 - \mu^*) d\Delta d\mu^* . \tag{71}$$

And again, as for Eq. (70):

$$K(E', E; \mu', \mu) = \int_{\beta_1^*}^{\beta_2^*} \sigma(E', E; \mu^*) \cdot \bar{I}^*(\mu^*; \mu', \mu) d\mu^* \quad (72)$$

Consequently the following relation holds:

$$\int_{\beta_1^*}^{\beta_2^*} \sigma(E', E; \mu^*) \cdot \bar{I}^*(\mu^*; \mu', \mu) d\mu^* = \sum_{i=1}^{IL} \sigma_i(E', \mu_{ci}^*) \cdot g_i(E') \cdot \bar{I}_i(\mu', \mu) \quad (73)$$

This relation can be transformed to show the equality by carrying out the integration over μ^* for the left hand side with use of Eq. (53). Thus, we have confirmed that the I^* -method is consistent with the I_i -method. But moreover, in the I^* -method double differential cross sections need not always be delta-functional (Eq. (53)). Therefore the I^* -method is more general than the I_i -method. The I_i -function depends on the scattering kinematics, while the I^* -function is free from scattering kinematics.

5.4 Discretization of the I^* -function

For discrete ordinate calculations we have again Eq. (21) for a spherical assembly:

$$\begin{aligned} & w_n \mu_n \left[A_{m+\frac{1}{2}} \cdot \bar{F}_g(m+\frac{1}{2}, n) - A_{m-\frac{1}{2}} \cdot \bar{F}_g(m-\frac{1}{2}, n) \right] + \\ & + \alpha_{n+\frac{1}{2}} \bar{F}_g(m, n+\frac{1}{2}) - \alpha_{n-\frac{1}{2}} \bar{F}_g(m, n-\frac{1}{2}) + w_n \cdot \sigma_t^* \cdot \bar{V}_m \cdot \bar{F}_g(m, n) = \quad (74) \\ & = w_n \bar{V}_m \left[C_g^{aniso}(m, n) + C_g^{iso}(m, n) \right] + w_n \cdot \bar{V}_m \cdot S_g(m, n) . \end{aligned}$$

where $S_g(m,n)$ is the external source, and

$$C_g^{aniso}(m,n) = \sum_{g'} \sum_{n'} \sigma_g^*(g'; n', n) \cdot \bar{F}_{g'}(m, n') \cdot W_{n'} \quad (75)$$

$$C_g^{iso} = \frac{1}{2} \sum_{g'} \sigma_{iso}(g', g) \sum_n F_{g'}(m, n) W_n \quad (76)$$

are the anisotropic and isotropic parts of the collision source.

The sink group anisotropic scattering matrix $\sigma_g^*(g'; n', n)$ is defined by

$$\begin{aligned} & \sigma_g^*(g'; n', n) = \\ & = \sum_{n_1^*}^{n_2^*} \left\{ \int_{\Delta E_{g'}} f_w(E') \int_{\Delta E_g} \int_{\Delta \mu_{n^*}} \sigma(E', E; \mu^*) \cdot T^*(\mu^*; n', n) d\mu^* dE dE' / \int f_w(E') dE' \Delta \mu_{n^*} \right\} \cdot W_{n^*} \end{aligned} \quad (77)$$

where n_1^* and n_2^* correspond to β_1^* and β_2^* .

$f_w(E)$ is the weighting function such as scalar flux spectra. The angular transfer probability function $T^*(\mu^*; n', n)$ is then discretized in an analogous way to the Ii-function, (Eq. (29) to (31)).

$$\begin{aligned} T^*(\mu^*; n', n) &= \frac{1}{2\pi W_n} \cdot \left[\arcsin(y_{n+\frac{1}{2}}^*) - \arcsin(y_{n-\frac{1}{2}}^*) \right] \quad \text{for } \beta_1^* < \mu^* < \beta_2^* \\ &= 0 \quad \text{for } \mu^* \leq \beta_1^* \text{ or } \mu^* \geq \beta_2^* \end{aligned} \quad (78)$$

with

$$y_{n \pm \frac{1}{2}}^* = \frac{\mu_{n \pm \frac{1}{2}} - \mu_{n'} \mu^*}{\sqrt{1 - \mu_n^2} \cdot \sqrt{1 - \mu^{*2}}} \quad (79)$$

If the double differential cross section data $\sigma(E', E; \mu^*)$, are given ^{*}) the processing code, which produces the scattering matrix, treats only the process of Eq. (77) with use of Eqs. (78) and (79), the I^{*}-function.

^{*}) We can also produce the double differential cross section from the partial (single differential) cross sections $\sigma_i(E', \mu_c)$ using Eq. (53).

If we separate the averaging for the double differential cross sections from the angular transfer probability function, we can use a fixed table for $T^*(n^*; n', n)$ by applying the same angle points μ_n for the three variables. Thus we get

$$G_g^*(g'; n', n) = \sum_{n_1^*}^{n_2^*} G(g', g; n^*) \cdot T^*(n^*; n', n) \cdot W_{n^*} \quad , \quad (80)$$

where

$$G(g', g; n^*) = \left[\int_{\Delta E_{g'}} f_w(E') \int_{\Delta E_g \Delta \mu_{n^*}} G(E', E; \mu^*) d\mu^* dE dE' \right] / \left[\Delta \mu_{n^*} \int_{\Delta E_{g'}} f_w(E') dE' \right]. \quad (81)$$

The matrix T^* is normalized in the sense that

$$\sum_{n_1^*}^{n_2^*} T^*(n^*; n', n) \cdot W_{n^*} = 1. \quad (82)$$

In Eq. (78) $\mu^* = \mu_{n^*}$ is used. This procedure is suitable for practical calculations. Eq. (80) means that we sum up the possible contributions of the angular transfer probability for the collision for fixed n' (incoming angle) and n (outcoming angle), by remarking the possible scattering angles n^* .

This procedure corresponds exactly to the S_N - P_∞ -calculation (see Appendix 2). In this I^* -method we have to carry out the summation with respect to n^* , instead of the calculation of P_L -coefficients and the summation of the polynomials in the P_L -method.

From the experience with the speed of the NITRAN-calculations we conclude that the calculational speed of the I^* -method will be high enough for practical calculations.

For two- or three-dimensional calculations we can also make a fixed table for Δ^* using

$$\Delta^*(n^*; n', n) = \arccos \frac{\mu_{n^*} - \mu_n \mu_{n'}}{\sqrt{1 - \mu_n^2} \sqrt{1 - \mu_{n'}^2}} \quad (83)$$

With this table we can calculate the collision source in a two- or three-dimensional transport problem without difficulty. Then the anisotropic collision source becomes:

$$\begin{aligned} (\text{coll. source})_g^{\text{aniso}} &= \\ &= \sum_{g'} \sum_{n'} \sum_{n^*} \sigma(g', g; n^*) \cdot T^*(n^*; n', n) \cdot f_{g'}(\vec{r}, n', \varphi + \Delta^*) \cdot W_{n^*} \cdot W_{n'} \end{aligned} \quad (84)$$

For two- or three-dimensional S_N -calculations, therefore, we must calculate the collision source directly with use of the double differential cross section and the angular transfer probability tables T^* and Δ^* . Within a S_N -code this is to be done inside the iteration loop for the sink energy group, the outer iteration loop. In Fig. 29 we present the proposed working scheme of a code system which realizes the I^* -method. Use of the "old" single differential data types must be foreseen, because the double differential data will certainly not be available for all materials.

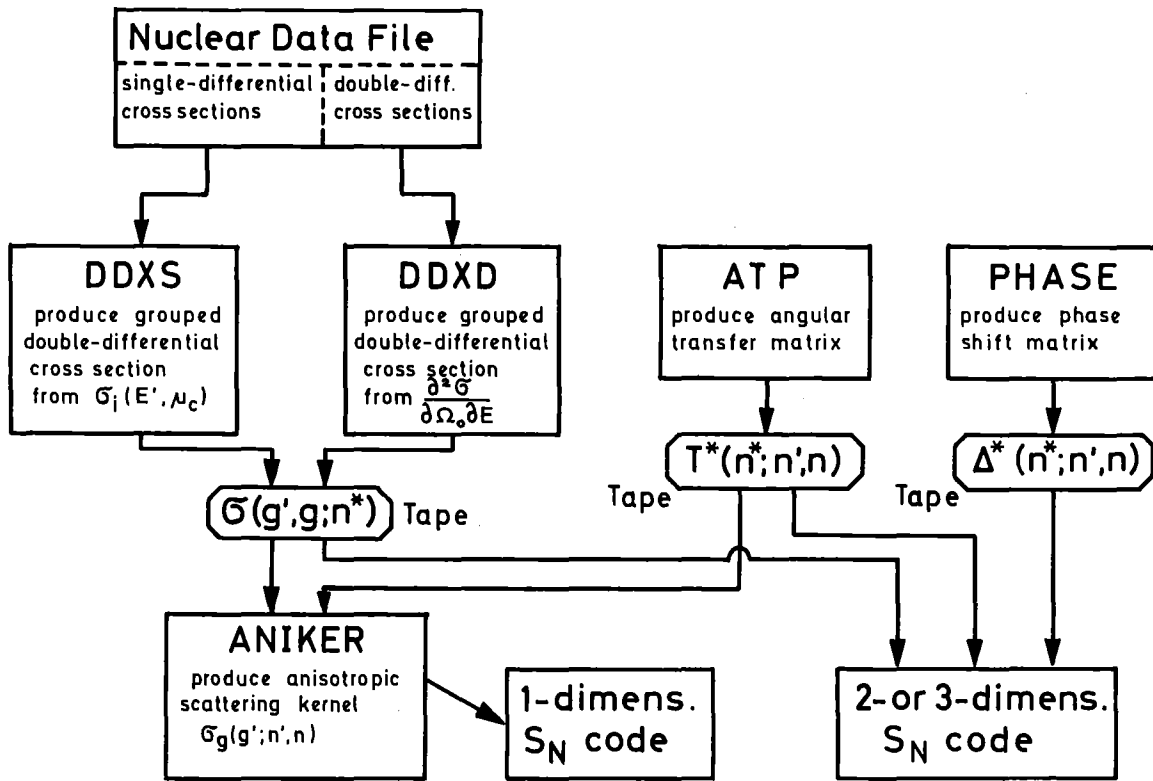


Fig. 29: Future system of neutron transport calculation by the I^* -method

The way in which we propose the use of double-differential cross sections is not the only one which we thought of. There is a more direct approach, starting from Eq. (68). When producing the kernel one can integrate the double differential cross section over an arbitrary phase shift $\Delta = \varphi' - \varphi$ and use Eq. (58). However, for the sake of methodical clearness we prefer the description of this section.

6. Conclusions

6.1 Conclusions with respect to accomplished work

We have presented two methods, the Ii- and the I*-method, for calculating the anisotropic collision source term for all types of scattering in a rigorous way. The following advantages are associated with these methods:

- a) We are free from approximations when calculating the anisotropic collision source. The discretization, e. g. in S_N -calculations, for numerical computation is the only approximation in these methods. Therefore, they can be references to test the accuracy of other methods, especially approximative methods like the P_L - or the T_{L+1} -method.
- b) Both methods provide an excellent tool to include the anisotropy of the non-elastic scattering into transport calculations.
- c) No negative fluxes are generated from the collision source term. This property makes these methods suited for the exponential interpolation scheme to produce the supplementary equations for the S_N -equation.
- d) When realizing the Ii-method by a one-dimensional code for spherical geometry, NITRAN-S, it was found that the calculational speed lies between that of P_3 - and P_5 calculations. Therefore the Ii-method is not only suited for accurate reference calculations, but also for practical application.

- e) The I^* -method is very promising, if the double differential neutron emission cross section in the LAB system is given. Unless these data exist in evaluated form, the I_i -method is used to reconstruct the double differential data from the partial data.

With respect to the flux and reaction rate calculation for fusion reactor neutronics we have to state the following:

- a) The effect of the anisotropy of the non-elastic scattering is not at all negligible.
- b) The effect of the transformation from the CM to the LAB system for non-elastic scattering is significant for light nuclei, even still for ^{12}C .

6.2 Conclusions with respect to future development

For the near future the existing code system NITRAN should be extended to have more feasibilities for technical use. In detail the extensions should be:

- a) The processing codes NIO and NIKER should accept more types of nuclear data.
- b) The interface code NIMIX to produce mixed-isotope-kernels for several material zones should be programmed.
- c) Various S_N -codes should be built for more geometries than only spherical: plane, cylindrical, two-dimensional, three-dimensional.

- d) NIO and NIKER should be connected to other S_N -codes, e. g. DTK.
- e) The Ii-method should be available also in the Monte-Carlo-calculations.

On a longer time scale the following extensions should be realized:

- a) The I^* -method should become the main tool for the neutron transport calculations. Therefore, the measurement and the evaluation of double-differential neutron emission cross sections, at least for the higher energies (above 2 MeV) must be stimulated.
- b) The Ii- and the I^* -method should be applied also to transport calculations for other particles than neutrons, especially at higher energies.

The nuclear data file KEDAK may easily be completed for fusion reactor application, because its alphanumeric declaration of data types is more open to new types than are the formats of ENDF/B. At least for the development of the I^* -method one can produce formally correct double differential neutron emission cross sections. This would introduce an element of continuity into the development of neutron transport calculations.

Finally, it must be stated that any useful assessment of errors for calculated quantities - here with respect to neutron transport problems - needs

- a) a rigorous calculational method for the neutron transport, and
- b) covariance data for the error estimate of the nuclear data together with a rigorous use of them for the error analysis.

Very often the double differential neutron emission cross section can be measured directly, especially at higher energies, and hence the covariance data can be given reliably. The present practice, however, is to construct partial cross sections with individual covariances (if at all). By this practice the requirements for the accuracies of the individual partial cross sections are unduly raised, if a given target accuracy of the neutron flux is to be met. Thus, again the I^* -method turns out to be best suited for the neutron transport part of the error analysis problem. For the second part of the problem the tools are to be developed. The sensitivity analysis method is a step into this direction [30]. This method should be extended to include also the effects of secondary neutron distributions with respect to angle and energy.

Looking backwards into the paper we find that the status of the nuclear data file is the most prominent obstacle on the way to neutron transport calculations with reliable error margins for the results.

Part II of this report is devoted to the realization of the I^* -method.

Acknowledgement

The authors would like to thank Prof. K. Wirtz, Dr. G. Keßler and DP M. Kichle for their support of the work. The encouragement accorded by Prof. K. Sumita of the Osaka University is also appreciated. We are indebted to Messrs. J. Yamamoto and K. Kasai of the Osaka University for their help in providing processed nuclear data, and to DP Stein for his advice in the use of KEDAK. We thank Drs. H. Küsters and E. Kiefhaber for the fruitful discussions. Thank is also due to Dr. F. Kappler for his friendly help concerning the understanding of the older DTK calculations.

One of the authors (A. T.) wishes to thank the Alexander-von-Humboldt-Stiftung for financially supporting his stay in the Institut für Neutronenphysik und Reaktortechnik of the Kernforschungszentrum Karlsruhe.

References

- /1/ R. Herzing, L. Kuijpers, P. Cloth, D. Filges,
R. Hecker, and N. Kirch
"Experimental and Theoretical Investigations
of Tritium Production in a Controlled Thermo-
nuclear Reactor Blanket Model"
Nucl.Sci.and Eng. 60, 169 (1976)
- /2/ L.J.M. Kuijpers
"Experimental Model Studies for a Fusion Reactor
Blanket"
PhD thesis Eindhoven, The Netherlands (1976)
also available as Jül 1356
- /3/ R. Herzing
"Erprobung neutronenphysikalischer Rechenver-
fahren an Lithiumblanketmodellen für einen
Fusionsreaktor"
PhD thesis Aachen, Fed.Rep. of Germany (1976)
available as Jül 1357
- /4/ P. Cloth, D. Filges, R. Herzing, N. Kirch
"Neutron Multiplication Effect of CTR Blankets Containing
Beryllium"
Proc. 9th Symp. on Fusion Technology (SOFT), Garmisch-
Partenkirchen, Fed. Rep. of Germany, June 14-18, (1976)
EUR 5602
- /5/ Y. Seki, H. Maekawa, M. Moriyama, T. Hiraoka
and J. Hirota
"Analysis of Fission Ratio Distribution in
Spherical Lithium Metal Assembly with a Graphite
Reflector"
JAERI-M-6220 (1975)

- /6/ H. Maekawa, Y. Seki
"Absolute Fission-Rate Distributions in Lithium and Hybrid Fusion Blanket Assemblies, I: Experimental Methods and Results, II: Analysis and Evaluation"
J. Nucl. Science and Technology 14 (1977) 97 and 210
- /7/ Engle, W.W.Jr.,
"A User's Manual for ANISN, a One-dimensional Discrete Ordinates Transport Code with Anisotropic Scattering"
K-1693, Union Carbide Corporation (1967)
- /8/ R.Q. Wright, N.M. Greene, J.L. Lucius, C.W. Craven, Jr.
"SUPERTOG, a Program to Generate Fine Group Constants and P_N -Scattering Matrices from ENDF/B"
ORNL-TM-2679 (1969)
- /9/ D.W. Muir (Los Alamos Scientific Lab.) private comm. to H. Seki
- /10/ R.E. MacFarlane, et al. Trans. ANS, 23 (1976) 16
- /11/ A. Takahashi, K. Iwai, J. Yamamoto, M. Ebisuya, K. Sumita
"Neutronics Experiments of D-T Fast Neutrons by Application of Associated Particle Method"
Journal Nucl. Sci. Techn. 14 (1977), 308
- /12/ M. Ebisuya, H. Maekawa, Y. Seki, A. Takahashi, J. Yamamoto
"A Study on the Neutron Transport Code Systems for Fusion Reactor Design",
JAERI-M 8135 (1979)
- /13/ A. Takahashi, J. Yamamoto, M. Ebisuya, K. Kasai, T. Ichida, K. Shintaku, K. Sumita
"Measurement of Angular Neutron Spectra Emitted from Fusion-Blanket Material Slabs, I: Experiment, II: Analysis" (in Japanese)
Trans. Fusion Conf. Tsukuba Feb. 1978
Section h-5, 6, (1978)

- /14/ H. Bachmann, U. Fritscher, F.W. Kappler, D. Rusch, H. Werle,
H.W. Wiese
"Neutron Spectra and Tritium Production Measurements on a
Lithium Sphere to Check Fusion Reactor Blanket Calculations"
Nucl. Sci. Eng. 67, 74 (1978)
- /15/ U. Fritscher, F. Kappler, D. Rusch
"Tritium Production Measurement in a Lithium Metal Sphere
with New Techniques in Neutron Source Strength Determination"
Nucl. Instr. and Meth. 153, 563, (1978)
- /16/ H.W. Wiese
"Verbesserte Behandlung der anisotropen elastischen Neutronen-
streuung durch konsistente Transportnäherungen energieabhän-
giger Ordnung"
PhD thesis, KFK 2377, Karlsruhe (1976)
- /17/ Memorandum of the IAEA Advisory Group Meeting on Nuclear Data
for Fusion Reactor Technology, 11 to 15 Dec. 1978, Vienna
- /18/ A. Takahashi, J. Yamamoto, M. Ebisuya, K. Sumita
"A Method for Calculating Anisotropic Neutron Transport
Using the Scattering Kernel without Polynomial Expansion"
Journal Nucl. Sci. and Technology, 16, No. 1, 1 (1979)
- /19/ K.D. Lathrop
"DTF-IV, A FORTRAN-IV Program for Solving the Multigroup
Transport Equation with Anisotropic Elastic Scattering"
LA-3373 (1965)
- /20/ C. Günther and W. Kinnebrock
"Das eindimensionale Transportprogramm DTK"
KFK 1381, Karlsruhe (1971)
- /21/ D. Woll
"GRUCAL, ein Programmsystem zur Berechnung
makroskopischer Gruppenkonstanten"
KFK 2108, Karlsruhe (1975)

- /22/ B. Goel
"Graphical Representation of the German Nuclear
Data Library KEDAK, Part 1, KFK 2233 or NEANDC(E)
170"U" 1975
- /23/ E. Stein (compiler); B. Krieg, I. Langner, R. Meyer, E. Stein
"The KEDAK Program Compendium. Part I to VI"
KFK 2387 I to VI, (1977 and 1978)
- /24/ P. Barbucci, F. Di Pasquantonio
"Exponential Supplementary Equations for S_N methods:
The One-Dimensional Case"
Nucl. Sci. Eng. 63, 179 (1977)
- /25/ ENDL - 73, Evaluated Nuclear Data Library, Lawrence Livermore
Laboratory (1973)
- /26/ D. Garber et al. BNL-400 (1970)
- /27/ D.M. Drake, G.F. Auchampaugh, E.D. Arthur, C.E. Ragan, P.G. Young
"Double-Differential Beryllium Neutron Cross Sections at
Incident Energies of 5.9, 10.1, and 14.2 MeV"
Nucl. Sci. Eng. 63, 401 (1977)
- /28/ H.H. Hogue, P.L. Von Behren, D.H. Epperson, S.G. Glendinning,
P.W. Lisowski, C.E. Nelson, H.W. Newson, F.O. Purser, W. Tornow,
C.R. Gould, L.W. Seagondollar
"Differential Elastic and Inelastic Scattering of 7- to 15-MeV
Neutrons from Beryllium"
Nucl. Sci. Eng. 68, 38 (1978)
- /29/ E. Greenspan and W.G. Price, Jr.
"Tritium Breeding Potential of the Princeton Reference Fusion
Power Plant"
MATT-1043, Princeton-University (1974)

- /30/ S.A.W. Gerstl, D.J. Dudziak, D.W. Muir
"Cross-Section Sensitivity and Uncertainty Analysis with
Application to a Fusion Reactor"
Nucl. Sci. Eng. 62, 137 (1977)
- /31/ S. Glasstone, M.C. Edlund
"The elements of nuclear reactor theory"
Van Nostrand, (1952)
- /32/ E.T. Whittaker, G.N. Watson
"A Course of Modern Analysis"
At the University Press, Cambridge, p. 327, (1958)
- /33/ J. B. Marion, J. L. Fowler
"Fast Neutron Physics, Part I",
Interscience Publishers Inc. New York (1960)
- /34/ J. P. Odom and J. K. Shultis
"Anisotropic neutron transport without Legendre expansions"
Nucl. Sci. Eng. 59, 278 (1976)

Appendix 1: Derivation of the Ii-function

The delta-functional representation of the scattering kernel, i. e. the double differential cross section for collisions of type i is written as (see also Appendix 2):

$$\sigma_i(g', g; \vec{\Omega}' \rightarrow \vec{\Omega}) = \frac{1}{2\pi} \cdot \sigma_i^{\circ}(g', g) \cdot \delta(\mu_o - \mu_i^*) , \quad (\text{A-1})$$

where the energy distribution of secondary neutrons, again only for the collisions of type i, is

$$\sigma_i^{\circ}(g', g) = \sigma_i(E_{g'}, \mu_{ci}^*) \cdot g_i(E_{g'}) \quad (\text{A-2})$$

with

μ_{ci}^* = scattering angle in the CM system

$\sigma_i(E_{g'}, \mu_{ci}^*)$ = differential cross section (from data table)

$g_i(E_{g'})$ = Jacobian for the collision of type i for incident energy $E_{g'}$, see Eq. (4)

The angle between the incident neutron vector $\vec{\Omega}$ and the outgoing neutron vector $\vec{\Omega}'$, see Fig. 7, is

$$\mu_o = \vec{\Omega}' \cdot \vec{\Omega} = \mu\mu' + \sqrt{1-\mu^2} \cdot \sqrt{1-\mu'^2} \cdot \cos(\varphi - \varphi') . \quad (\text{A-3})$$

This is, however, not a free variable. Eq. (A-1) means that the scattering angle is fixed to the particular value of μ_i^* , which is defined by the scattering kinematics, i. e. $E_{g'}$, E_g , Q_i , and A. The collision source for scattering of type i is written by summing up the neutrons coming from $(E_{g'}, \mu', \varphi')$ to (E_g, μ, φ) at a given position \vec{r}

$$(\text{coll. source})_{g,i} = \sum_{g'} \int_{-1}^{+1} \sigma_i^{\circ}(g', g) \cdot \frac{1}{2\pi} \int_0^{2\pi} \delta(\mu_o - \mu_i^*) \cdot f_{g'}(\vec{r}, \mu', \varphi') d\varphi' d\mu' . \quad (\text{A-4})$$

We transform the variables as follows, in order to carry out the integration over φ' :

$$X_0 = \sqrt{1-\mu^2} \cdot \sqrt{1-\mu'^2} \quad (\text{A-5})$$

$$X = X_0 \cdot \cos(\varphi - \varphi') \quad (\text{A-6})$$

The integration over $[0, 2\pi]$ in φ' -space being equal to the integration over $[\varphi, 2\pi + \varphi]$ Eq. (A-4) is transformed as follows:

$$\begin{aligned} (\text{coll. source})_{g,i} &= \\ &= \sum_{g'=-1}^{+1} \int_{g'=-1}^{+1} \sigma_i^0(g', g) \cdot \frac{1}{\pi} \int_{-X_0}^{X_0} \frac{1}{\sqrt{X_0^2 - X^2}} \cdot \delta(\mu\mu' - \mu_i^* + X) \cdot f_{g'}(\vec{r}, \mu', \varphi + \arccos(\frac{X}{X_0})) dX d\mu' \quad (\text{A-7}) \end{aligned}$$

We can carry out the integration over X and get:

$$\begin{aligned} (\text{coll. source})_{g,i} &= \\ &= \sum_{g'=-1}^{+1} \int_{g'=-1}^{+1} \sigma_i^0(g', g) \cdot I_i(\mu', \mu) \cdot f_{g'}(\vec{r}, \mu', \varphi + \Delta_i^*) d\mu' \quad (\text{A-8}) \end{aligned}$$

where $I_i(\mu', \mu)$ is given, by setting $X = \mu_i^* - \mu\mu'$ in $\sqrt{X_0^2 - X^2}$, as:

$$\begin{aligned} I_i(\mu', \mu) &= \frac{1}{\pi \sqrt{1-\mu^2-\mu'^2-\mu_i^{*2} + 2\mu\mu'\mu_i^*}} \quad \text{for } \beta_1 < \mu < \beta_2, \\ &= 0 \quad \text{for } \mu \leq \beta_1 \text{ or } \mu \geq \beta_2 \text{ with } |\mu| \neq 1, |\mu'| \neq 1, |\mu_i^*| \neq 1. \quad (\text{A-9}) \end{aligned}$$

The phase shift Δ_i^* in the collision (in φ -space) is given as (again $X = \mu_i^* - \mu\mu'$)

$$\Delta_i^* = \arccos \left[\frac{\mu_i^* - \mu\mu'}{\sqrt{1-\mu^2} \sqrt{1-\mu'^2}} \right] \quad (\text{A-10})$$

for $|\mu| \neq 1$, $|\mu'| \neq 1$, and $|\mu_i^*| \neq 1$

For the cases of $|\mu| = 1$ or $|\mu'| = 1$ or $|\mu_i| = 1$ the delta-functional kernel (Eq. (A-1)) becomes independent of φ' . For these extreme cases we get firstly:

$$(coll. source)_{g,i} = \sum_{g'=-1}^{+1} \int \sigma_i^o(g',g) \cdot \delta(\mu\mu' - \mu_i^*) \cdot \frac{1}{2\pi} \int_0^{2\pi} f_{g'}(\vec{r}_i, \mu', \varphi') d\varphi' d\mu' \quad (A-11)$$

if $|\mu| = 1$ or $|\mu'| = 1$.

Secondly: $\Delta_i^* = 0$

$$I_i(\mu', \mu) = \delta(\mu - \mu' \mu_i^*) \quad (A-12)$$

if $|\mu_i^*| = 1$, and $|\mu| \neq 1$, $|\mu'| \neq 1$.

For discretized calculations (e. g. S_N) we need only the representations (A-9) and (A-10) for the calculation of the angular transfer probability. In calculations with continuous variables, e. g. Monte-Carlo, the representation of the extreme cases must be included.

Appendix 2: Scattering kinematics and kernel

A 2.1 Scattering kinematics

After the collision the target nucleus is excited to an energy Q_i , which may be $Q_1 = 0$ for elastic scattering, Q_2, Q_3 , etc. for discrete level excitation, and some other value for continuum scattering. The conservation of energy and momentum yields the two equations

$$\frac{1}{2} (v_1^c)^2 + \frac{1}{2} A (V_1^c)^2 = \frac{1}{2} \left(\frac{A}{A+1}\right)^2 (v')^2 + \frac{A}{2} \left(\frac{v'}{A+1}\right)^2 - Q_i \quad (A-13)$$

$$v_1^c + A V_1^c = 0 \quad (A-14)$$

where v' is the incident neutron velocity in the Laboratory (LAB) system corresponding to the incident energy E' . v_1^c is the neutron velocity in the center of mass (CM) system after the collision, V_1^c the velocity of the recoil nucleus in the CM system, and A the mass of the nucleus relative to the neutron. Replacing v' , v_1^c , and V_1^c by energies we get:

$$\frac{E}{E'} = \frac{A^2(1 - Q_i/E^*) + 1 + 2A\mu_c'}{(A+1)^2} \quad (\text{A-15})$$

where E is the neutron energy after the collision and μ_c the scattering angle in the CM system. μ_c' is an abbreviation:

$$\mu_c' = \mu_c \cdot \sqrt{1 - Q_i/E^*} \quad (\text{A-16})$$

and E^* is another one:

$$E^* = \frac{A}{A+1} \cdot E' \quad (\text{A-17})$$

For μ_o , the scattering angle in the LAB system, we get:

$$\mu_o = \frac{1 - A\mu_c'}{\sqrt{1 + 2A\mu_c' + A^2(1 - Q_i/E^*)}} \quad (\text{A-18})$$

For μ_c :

$$\mu_c = \frac{\frac{(A+1)^2}{2A} \cdot \frac{E}{E'} - \frac{A}{2} \cdot (1 - Q_i/E^*) - \frac{1}{2A}}{\sqrt{1 - Q_i/E^*}} \quad (\text{A-19})$$

Replacing the abbreviation μ_c' in Eq. (A-18) by (A-16) and substituting μ_c from Eq. (A-19) we obtain:

$$\mu_o = \frac{1}{2} \left\{ (A+1) \sqrt{\frac{E}{E'}} - \frac{1}{A+1} \cdot [A^2(1 - Q_i/E^*) - 1] \cdot \sqrt{\frac{E'}{E}} \right\}. \quad (\text{A-20})$$

A 2.2 Scattering kernel

The scattering kernel (double-differential cross section) $\sigma_i(E' \rightarrow E, \Omega' \rightarrow \Omega)$ in the laboratory system is

$$\sigma_i(E' \rightarrow E, \vec{\Omega}' \rightarrow \vec{\Omega}) = \frac{1}{2\pi} \sigma_i(E', \mu_o) \delta(\mu_o - \mu_i^*(E', E)) \cdot \left| \frac{\partial \mu_o}{\partial E} \right|. \quad (\text{A-21})$$

As $\mu_o = \mu_i(E', E)$, we get $\frac{\partial \mu_o}{\partial E}$ by differentiating the right hand side of Eq. (A-20):

$$\left| \frac{\partial \mu_o}{\partial E} \right| = \frac{1}{4E} \left\{ (A+1) \sqrt{\frac{E'}{E}} + \frac{1}{A+1} [A^2(1-Q_i/E^*) - 1] \sqrt{\frac{E'}{E}} \right\}. \quad (\text{A-22})$$

The differential cross section is usually given in the CM system, $\sigma_i(E', \mu_c)$. The relation between $\sigma_i(E', \mu_c)$ and $\sigma_i(E', \mu_o)$ is

$$\sigma_i(E', \mu_o) = \sigma_i(E', \mu_c) \cdot \left| \frac{\partial \mu_c}{\partial \mu_o} \right| \quad (\text{A-23})$$

To get the derivative $\frac{\partial \mu_c}{\partial \mu_o}$, we use the relation between μ_c and μ_o , which we obtain from Eqs. (A-15), (A-18), (A-19) and (A-20):

$$\mu_c = \frac{1}{A \sqrt{1-Q_i/E^*}} \left\{ \mu_o^2 - 1 + \mu_o \sqrt{\mu_o^2 - 1 + A^2(1-Q_i/E^*)} \right\}. \quad (\text{A-24})$$

Hence

$$\begin{aligned} \left| \frac{\partial \mu_c}{\partial \mu_o} \right| &= \\ &= 2 \cdot \sqrt{1-Q_i/E^*} \cdot \left(\frac{A+1}{A} \right)^2 \cdot \frac{E'}{E'} \left/ \left\{ \frac{A+1}{A} \cdot \sqrt{\frac{E'}{E}} + \frac{1}{A(A+1)} [A^2(1-Q_i/E^*) - 1] \cdot \sqrt{\frac{E'}{E}} \right\} \right. \end{aligned} \quad (\text{A-25})$$

We define the function $g_i(E')$, the "Jacobian", as follows:

$$g_i(E') = \left| \frac{\partial \mu_o}{\partial E} \right| \cdot \left| \frac{\partial \mu_c}{\partial \mu_o} \right| \quad (\text{A-26})$$

with Eqs. (A-22) and (A-25) we obtain:

$$g_i(E') = \frac{2}{(1-\alpha) \cdot E' \cdot \sqrt{1-Q_i/E^*}} \quad (\text{A-27})$$

with the abbreviations $\alpha = (A-1)^2/(A+1)^2$ and $E^* = E' \cdot A/(A+1)$.

For elastic scattering, ($Q_i = 0$), $g_i(E')$ is the well known slowing-down kernel for isotropic scattering in the CM system. For the general case we rewrite the scattering kernel Eq. (A-21) with the Jacobian g_i .

$$G_i(E' \rightarrow E, \vec{\Omega}' \rightarrow \vec{\Omega}) = \frac{1}{2\pi} G_i(E', \mu_c) \cdot g_i(E') \cdot \delta(\mu_0 - \mu_i^*(E', E)). \quad (A-28)$$

The total scattering kernel is produced by summing up all partial kernels

$$G(E' \rightarrow E, \vec{\Omega}' \rightarrow \vec{\Omega}) = \sum_{i=1}^{IL} G_i(E' \rightarrow E, \vec{\Omega}' \rightarrow \vec{\Omega}). \quad (A-29)$$

In the initial phase of the development of the new method the summing of kernels referred only to level scattering, now the continuum scattering is included.

A 2.3 Legendre polynomial expansion of the scattering kernel

The Legendre polynomial expansion of the scattering kernel is written as [31]:

$$G_i(E' \rightarrow E, \vec{\Omega}' \rightarrow \vec{\Omega}) = \frac{1}{4\pi} \sum_{\ell=0}^{\infty} G_i^{\ell}(E', E) \cdot P_{\ell}(\mu_0). \quad (A-30)$$

The n-th component of the series is obtained by multiplying Eq. (A-30)

with $P_n(\mu_0)$ and integrating over μ_0 :

$$\int_{-1}^{+1} G_i(E' \rightarrow E, \vec{\Omega}' \rightarrow \vec{\Omega}) d\mu_0 = \frac{1}{4\pi} \int_{-1}^{+1} \sum_{\ell=0}^{\infty} G_i^{\ell}(E', E) \cdot P_{\ell}(\mu_0) \cdot P_n(\mu_0) d\mu_0 \quad (A-31)$$

The absolute convergence of the series allows exchange of summation and integration. Then with use of the orthogonality of the Legendre polynomials, i. e.

$$\begin{aligned} \frac{2n+1}{2} \int_{-1}^{+1} P_m(\mu) \cdot P_n(\mu) d\mu &= 1 \quad \text{for } m=n \\ &= 0 \quad \text{for } m \neq n, \end{aligned} \quad (\text{A-32})$$

we get:

$$\bar{G}_i^n(E', E) = \frac{2n+1}{2} \cdot 4\pi \int_{-1}^{+1} \bar{G}_i(E' \rightarrow E, \vec{\Omega}' \rightarrow \vec{\Omega}) \cdot P_n(\mu_0) d\mu_0. \quad (\text{A-33})$$

Inserting $\sigma_i(E' \rightarrow E, \vec{\Omega}' \rightarrow \vec{\Omega})$ from Eq. (A-28) into (A-33):

$$\bar{G}_i^n(E', E) = (2n+1) \int_{-1}^{+1} \bar{G}_i(E', \mu_c) \cdot g_i(E') \cdot \delta(\mu_0 - \mu_i^*(E', E)) \cdot P_n(\mu_0) d\mu_0. \quad (\text{A-34})$$

In this integration μ_c is no longer a free variable. It is fixed by the δ -function and the kinematic equations Eqs. (A-15), (A-18), and (A-19). Therefore the integration yields:

$$\bar{G}_i^n(E', E) = (2n+1) \cdot \bar{G}_i(E', \mu_{ci}^*) \cdot g_i(E') \cdot P_n(\mu_i^*). \quad (\text{A-35})$$

μ_{ci}^* is given by the right hand side of Eq. (A-19), and μ_i^* by the right hand side of Eq. (A-20) for the same reasons. Eq. (A-35) can be transformed another time by the use of Eq. (A-2), which in the form of continuous variables becomes:

$$\bar{G}_i^0(E', E) = \bar{G}_i(E', \mu_{ci}^*) \cdot g_i(E'). \quad (\text{A-36})$$

Thus we have:

$$\bar{G}_i^n(E', E) = (2n+1) \cdot P_n(\mu_i^*) \cdot \bar{G}_i^0(E', E). \quad (\text{A-37})$$

Eq. (A-37) means that we can obtain the coefficients $\sigma_i^{\ell}(E',E)$, if only $\sigma_i^0(E',E)$ is given. The coefficients $\sigma_i^{\ell}(E',E)$ are called the " P_{ℓ} -kernels", especially $\sigma_i^0(E',E)$ the " P_0 -kernel". In the " P_L -method" the Legendre polynomial expansion of the scattering kernel, Eq. (A-30), is truncated at the L -th term. It is the characteristic of Eq. (A-37), which has caused the wide-spread use of the P_L -method. In the "improved" P_L -methods, for instance in the T_{L+1} -method /16/, an estimate for the rest of the series is introduced.

Appendix 3: Relation between the I^* - and the P_L -method

In the P_L -method the expansion of the scattering kernel, Eq. (A-30), is truncated at the L -th term:

$$G(E',E; \vec{\Omega}', \vec{\Omega}) = \frac{1}{4\pi} \sum_{\ell=0}^L G^{\ell}(E',E) \cdot P_{\ell}(\mu^*). \quad (\text{A-38})$$

We have omitted the index i for the collision type and write μ^* for the scattering angle without distinguishing between μ_0 and μ^* .

We change the notation for the kernel using the following relation:

$$G(E',E; \vec{\Omega}', \vec{\Omega}) = \frac{1}{2\pi} G(E',E; \mu^*) \quad (\text{A-39})$$

which is the final form of Eq. (50) in section 5. Thus we get:

$$G(E',E; \mu^*) = \frac{1}{2} \sum_{\ell=0}^L G^{\ell}(E',E) \cdot P_{\ell}(\mu^*). \quad (\text{A-40})$$

In the same way as in Appendix 2 the ℓ -th coefficient of the series is given by

$$G^\ell(E', E) = (2\ell+1) \int_{-1}^{+1} G(E', E; \mu^*) \cdot P_\ell(\mu^*) d\mu^*. \quad (A-41)$$

We transcribe Eq. (A-40) with use of the addition theorem for the Legendre polynomials [32]:

$$G(E', E; \mu^*) = \frac{1}{2} \sum_{\ell=0}^L G^\ell(E', E) \cdot \left\{ P_\ell(\mu') \cdot P_\ell(\mu) + 2 \sum_{m=1}^{\ell} \frac{(\ell-m)!}{(\ell+m)!} \cdot P_\ell^m(\mu') \cdot P_\ell^m(\mu) \cdot \cos(m \cdot (\varphi' - \varphi)) \right\}. \quad (A-42)$$

The collision source term in the transport equation for the one-dimensional case in the discretized form with group-averaged cross sections is written as [7], [16], [19]:

$$\begin{aligned} (\text{coll. source})_g^{\text{aniso}} &= \\ &= \sum_{g'} \frac{1}{2} \sum_{\ell=0}^L G^\ell(E_{g'}, E_g) \cdot \frac{1}{2\pi} \int_0^{2\pi} \int_{-1}^{+1} P_\ell(\mu^*) f_{g'}(\tau, \mu', \varphi') d\mu' d\varphi' \end{aligned} \quad (A-43)$$

Replacing that part of this equation, which corresponds to the right hand side of Eq. (A-40) by the more complicated expression Eq. (A-42) we can integrate over φ . As we integrate over full periods of the cosine, all terms vanish except for the first:

$$\int_0^{2\pi} (\text{coll. source})_g^{\text{aniso}} d\varphi = \sum_{g'} \frac{1}{2} \sum_{\ell=0}^L G^\ell(E_{g'}, E_g) \cdot P_\ell(\mu) \int_{-1}^{+1} P_\ell(\mu') \cdot F_{g'}(\tau, \mu') d\mu' \quad (A-44)$$

with

$$\bar{F}_{g'}(\tau, \mu') = \int_0^{2\pi} f_{g'}(\tau, \mu', \varphi') d\varphi'. \quad (A-45)$$

Inserting $\sigma^{\ell}(E_{g_1}, E_g)$ from Eq. (A-41) into (A-44) we get:

$$\int_0^{2\pi} (\text{coll. source})_g^{\text{aniso}} d\varphi =$$

$$= \sum_{g'} \int_{-1}^{+1} \int_{-1}^{+1} \sigma(E_{g_1}, E_g; \mu^*) \left\{ \frac{1}{2} \sum_{\ell=0}^L (2\ell+1) P_{\ell}(\mu^*) \cdot P_{\ell}(\mu') \cdot P_{\ell}(\mu) \right\} F_{g'}(\tau, \mu') d\mu^* d\mu' \quad (\text{A-46})$$

Comparing this equation with Eq. (60) of section 5 we notice that the angular transfer probability T_L in the P_L -method is expressed by:

$$T_L(\mu^*; \mu', \mu) = \frac{1}{2} \sum_{\ell=0}^L (2\ell+1) P_{\ell}(\mu^*) P_{\ell}(\mu') \cdot P_{\ell}(\mu) \quad (\text{A-47})$$

As the series Eq. (A-30) represents the identical starting point for both the I^* - and the P_L -method, we find that $T_L(\mu^*; \mu', \mu)$ converges against $T^*(\mu; \mu', \mu)$ for $L \rightarrow \infty$, because convergence is assured at all stages of the derivation of T_L .

In general coordinates we have the original form of the collision source term in the I^* -method:

$$(\text{coll. source})_g^{\text{aniso}}$$

$$= \frac{1}{2\pi} \sum_{g'} \int_{\Omega'} \int_{-1}^{+1} \sigma(E_{g_1}, E_g; \mu^*) \cdot \delta(\mu_0 - \mu^*) \cdot f_{g'}(\vec{r}, \vec{\Omega}') d\mu^* d\Omega' \quad (\text{A-48})$$

If we use the Legendre polynomial expansion of the delta-function, i. e.

$$\delta(\mu_0 - \mu^*) = \frac{1}{2} \sum_{\ell=0}^{\infty} (2\ell+1) P_{\ell}(\mu^*) \cdot P_{\ell}(\mu_0) \quad (\text{A-49})$$

the collision source is rewritten as

$$(\text{coll. source})_g^{\text{aniso}}$$

$$= \frac{1}{4\pi} \sum_{g'} \int_{\Omega'} \sum_{\ell=0}^{\infty} (2\ell+1) \left\{ \int_{-1}^{+1} \sigma(E_{g_1}, E_g; \mu^*) P_{\ell}(\mu^*) d\mu^* \right\} P_{\ell}(\mu_0) f_{g'}(\vec{r}, \vec{\Omega}') d\Omega' \quad (\text{A-50})$$

Using the equation for the determination of the P_ℓ -coefficients, Eq. (A-41), the collision source representation is transformed into that of the P_L -method for $L \rightarrow \infty$:

$$(\text{coll. source})_g^{\text{aniso}} = \frac{1}{4\pi} \sum_{g'} \sum_{\ell=0}^{\infty} \sigma^\ell(E_g, E) \int_{\Omega'} P_\ell(\mu_0) f_{g'}(\vec{r}, \vec{\Omega}') d\Omega' \quad (\text{A-51})$$

Thus, we have confirmed that the I^* -method is equivalent to P_∞ not only for the one-dimensional case, but also for general coordinates.

Table 1

67 - GROUP NEUTRON ENERGY GROUP STRUCTURE

GROUP	ENERGY (TCP,LCW,MIC)			ENERGY-WIDTH LETHARGY-WIDTH	
1	1.500000E+01	1.473500E+01	1.486749E+01	2.6500034E-01	1.7824583E-02
2	1.473500E+01	1.447400E+01	1.460450E+01	2.6099968E-01	1.7871425E-02
3	1.447400E+01	1.421800E+01	1.434599E+01	2.5599957E-01	1.7844260E-02
4	1.421800E+01	1.396700E+01	1.409249E+01	2.5100040E-01	1.7810531E-02
5	1.396700E+01	1.372000E+01	1.384349E+01	2.4699974E-01	1.7842382E-02
6	1.372000E+01	1.347700E+01	1.359849E+01	2.4300033E-01	1.7869551E-02
7	1.347700E+01	1.323900E+01	1.335799E+01	2.3799992E-01	1.7817091E-02
8	1.323900E+01	1.300500E+01	1.312199E+01	2.3400021E-01	1.7813013E-02
9	1.300500E+01	1.277500E+01	1.288999E+01	2.3000050E-01	1.7843321E-02
10	1.277500E+01	1.254900E+01	1.266199E+01	2.2599983E-01	1.7848942E-02
11	1.254900E+01	1.218200E+01	1.236549E+01	3.6699963E-01	2.9680751E-02
12	1.218200E+01	1.182500E+01	1.200349E+01	3.5700035E-01	2.9742781E-02
13	1.182500E+01	1.147900E+01	1.165199E+01	3.4599972E-01	2.9696491E-02
14	1.147900E+01	1.114300E+01	1.131099E+01	3.3600044E-01	2.9707603E-02
15	1.114300E+01	1.081700E+01	1.097999E+01	3.2599926E-01	2.9691864E-02
16	1.081700E+01	1.050000E+01	1.065849E+01	3.1700039E-01	2.9743705E-02
17	1.050000E+01	1.008900E+01	1.029449E+01	4.1100025E-01	3.9929260E-02
18	1.008900E+01	9.692999E+00	9.895999E+00	3.9599991E-01	4.0041048E-02
19	9.692999E+00	9.314000E+00	9.503499E+00	3.7899971E-01	3.5885279E-02
20	9.314000E+00	8.949000E+00	9.131500E+00	3.6499977E-01	3.9975993E-02
21	8.949000E+00	8.597999E+00	8.773499E+00	3.5100079E-01	4.0011730E-02
22	8.597999E+00	8.260000E+00	8.429499E+00	3.3699989E-01	3.9983325E-02
23	8.260000E+00	7.937999E+00	8.099499E+00	3.2299995E-01	3.9883442E-02
24	7.937999E+00	7.626999E+00	7.782499E+00	3.1099997E-01	3.9965913E-02
25	7.626999E+00	7.326999E+00	7.476999E+00	3.0000019E-01	4.0128089E-02
26	7.326999E+00	7.041000E+00	7.184000E+00	2.8599993E-01	3.9815627E-02
27	7.041000E+00	6.765000E+00	6.902999E+00	2.7600002E-01	3.9987907E-02
28	6.765000E+00	6.500000E+00	6.632499E+00	2.6500034E-01	3.9959498E-02
29	6.500000E+00	6.241999E+00	6.370999E+00	2.5800037E-01	4.0500898E-02
30	6.241999E+00	5.994999E+00	6.118499E+00	2.4699974E-01	4.0374506E-02
31	5.994999E+00	5.757000E+00	5.875999E+00	2.3799992E-01	4.0509138E-02
32	5.757000E+00	5.529000E+00	5.642999E+00	2.2799960E-01	4.0409312E-02
33	5.529000E+00	5.310000E+00	5.419500E+00	2.1899986E-01	4.0414806E-02
34	5.310000E+00	5.099000E+00	5.204500E+00	2.1100044E-01	4.0546685E-02
35	5.099000E+00	4.897000E+00	4.993000E+00	2.0199966E-01	4.0421221E-02
36	4.897000E+00	4.703000E+00	4.800000E+00	1.9400024E-01	4.0422134E-02
37	4.703000E+00	4.515999E+00	4.609499E+00	1.8700027E-01	4.0573243E-02
38	4.515999E+00	4.336999E+00	4.426499E+00	1.7899990E-01	4.0443201E-02
39	4.336999E+00	4.165000E+00	4.250999E+00	1.7199993E-01	4.0466093E-02
40	4.165000E+00	4.000000E+00	4.082499E+00	1.6499996E-01	4.0421221E-02
41	4.000000E+00	3.849000E+00	3.849499E+00	3.0099964E-01	7.8231692E-02
42	3.849000E+00	3.418999E+00	3.590000E+00	2.8000069E-01	7.8714013E-02
43	3.418999E+00	3.161999E+00	3.290499E+00	2.5699997E-01	7.8142643E-02
44	3.161999E+00	2.923999E+00	3.042999E+00	2.3799992E-01	7.8252017E-02
45	2.923999E+00	2.704000E+00	2.814000E+00	2.1999993E-01	7.8219354E-02
46	2.704000E+00	2.500000E+00	2.602000E+00	2.0400047E-01	7.8441620E-02
47	2.500000E+00	2.270000E+00	2.385000E+00	2.2999954E-01	9.6510589E-02
48	2.270000E+00	2.060000E+00	2.165499E+00	2.0900059E-01	9.6538492E-02
49	2.060000E+00	1.871000E+00	1.965999E+00	1.8999990E-01	9.6717477E-02
50	1.871000E+00	1.698000E+00	1.784500E+00	1.7300034E-01	9.7021341E-02
51	1.698000E+00	1.541999E+00	1.619999E+00	1.5600014E-01	9.6370280E-02
52	1.541999E+00	1.399999E+00	1.470999E+00	1.4200020E-01	9.6607566E-02
53	1.399999E+00	1.274999E+00	1.337499E+00	1.2500007E-01	9.3525529E-02
54	1.274999E+00	1.161999E+00	1.218499E+00	1.1299992E-01	9.2802703E-02
55	1.161999E+00	1.057999E+00	1.109999E+00	1.0400009E-01	9.3761802E-02
56	1.057999E+00	9.639999E-01	1.010999E+00	9.3999624E-02	9.3043447E-02
57	9.639999E-01	8.790000E-01	9.210000E-01	8.5999966E-02	9.3443930E-02
58	8.790000E-01	8.000000E-01	8.389999E-01	7.8000009E-02	9.3034685E-02
59	8.000000E-01	7.130000E-01	7.564999E-01	8.7000012E-02	1.1512959E-01
60	7.130000E-01	6.349999E-01	6.739999E-01	7.8000009E-02	1.1585605E-01
61	6.349999E-01	5.659999E-01	6.004999E-01	6.9000006E-02	1.1503017E-01
62	5.659999E-01	5.040000E-01	5.349999E-01	6.1599997E-02	1.1601740E-01
63	5.040000E-01	4.490000E-01	4.764999E-01	5.5000007E-02	1.1555278E-01
64	4.490000E-01	3.999999E-01	4.244999E-01	4.9000025E-02	1.1555785E-01
65	3.999999E-01	3.560000E-01	3.779999E-01	4.3999970E-02	1.1653358E-01
66	3.560000E-01	3.169999E-01	3.364999E-01	3.9000034E-02	1.1602843E-01
67	3.169999E-01	1.000000E-02	1.624999E-01	3.0699992E-01	3.4563160E+00

Table 2 μ -points for S_{32} calculation

<u>n</u>	<u>μ_n</u>	<u>W_n</u>
1	- 0.99990	4.0000E-4
2	- 0.99850	1.2250E-3
3	- 0.99500	1.7500E-3
4	- 0.99150	2.5500E-3
5	- 0.98480	5.3750E-3
6	- 0.97000	8.4350E-3
7	- 0.95106	1.1250E-2
8	- 0.92500	1.5265E-2
9	- 0.89000	2.6250E-2
10	- 0.82000	4.7500E-2
11	- 0.70000	6.1625E-2
12	- 0.57350	6.2500E-2
13	- 0.45000	6.3375E-2
14	- 0.32000	7.2500E-2
15	- 0.16000	6.7500E-2
16	- 0.05000	5.2500E-2
17	0.05000	5.2500E-2
18	0.16000	6.7500E-2
19	0.32000	7.2500E-2
20	0.45000	6.3375E-2
21	0.57350	6.2500E-2
22	0.70000	6.1625E-2
23	0.82000	4.7500E-2
24	0.89000	2.6250E-2
25	0.92500	1.5265E-2
26	0.95106	1.1250E-2
27	0.97000	8.4350E-3
28	0.98480	5.3750E-3
29	0.99150	2.5500E-3
30	0.99500	1.7500E-3
31	0.99850	1.2250E-3
32	0.99990	4.0000E-4